Localized Effects of Hurricane Michael (2018) on Total Electron Content

THESIS

Joanna E. S. Williams, Capt, USAF

AFIT-ENP-MS-20-M-122

DEPARTMENT OF THE AIR FORCE
AIR UNIVERSITY

AIR FORCE INSTITUTE OF TECHNOLOGY

Wright-Patterson Air Force Base, Ohio

AFIT-ENP-MS-20-M-122

LOCALIZED EFFECTS OF HURRICANE MICHAEL (2018) ON TOTAL ELECTRON CONTENT

THESIS

Presented to the Faculty

Department of Engineering Physics

Graduate School of Engineering and Management

Air Force Institute of Technology

Air University

Air Education and Training Command

in Partial Fulfillment of the Requirements for the

Degree of Master of Science in Atmospheric Science

Joanna E. S. Williams, B.S.

Capt, USAF

March 2020

AFIT-ENP-MS-20-M-122

LOCALIZED EFFECTS OF HURRICANE MICHAEL (2018) ON TOTAL ELECTRON CONTENT

THESIS

Joanna E. S. Williams, B.S.
Capt, USAF

Committee Membership:

Lt Col Omar A. Nava, Ph.D.
Chair

Lt Col Robert C. Tournay, Ph.D.
Member

Lt Col H. Rose Tseng, Ph.D.
Member

Maj Daniel J. Emmons, Ph.D.
Member

Abstract

Understanding the connection between terrestrial and space environments is an emerging field of study that can significantly improve operational weather forecasting. In particular, it is well known that tropical cyclones (TCs) and thunderstorms can initiate gravity waves that generate fluctuations in the total electron content (TEC) of the ionosphere. These perturbations can deteriorate and delay the transmission of high-frequency (HF) communications, such as emergency services, amateur radio, and aviation. This study investigates changes in TEC according to the number of lightning flashes and the rainfall rates associated with Hurricane Michael (2018). A composite analysis will be performed using the GOES Geostationary Lightning Mapper (GLM), NCEP Stage IV Precipitation, and Massachusetts Institute of Technology (MIT) Haystack's Global Positioning System (GPS) TEC data sets to characterize the influence of lightning on the ionosphere at Hurricane Michael's peak intensity on 10 October 2018. Overall, improved characterization of the dynamic and electrodynamic connection between the lower and upper atmospheres has important implications for both space physics and atmospheric science communities. The techniques developed in this study have the potential to improve forecasting of tropical cyclogenesis, tropical cyclone intensification, and the discrimination between naturogenic and anthropogenic phenomena impacts on the ionosphere. No correlation is found between lightning and TEC variations; however, there are some more conclusive results relating a moderate rainfall rate to an increase in TEC variation during Hurricane Michael.

Acknowledgements

First, I would like to thank my husband for never-ending support and encouragement throughout this 18-month program. Although he may not be here with me, his loving dedication has bolstered my motivation through tasks, assignments, and sleepless nights. I would not be here today without him.

I would like to thank my mother and siblings for their confidence and inspiration to follow and pursue my ambitions now and through the past 26 years. They have been the backbone to my accomplishments thus far.

I could not have completed this without the tireless assistance and guidance from my committee. Throughout the process, each member has helped with keeping me on track, especially if I was heading in the wrong direction. Thank you for taking the time out of your busy schedules to assist and advise me through this project.

Finally, I would like to thank my classmates for enduring and pressing through the journey of AFIT with me. All of this would not have been possible without the support and encouragement through the ups and downs of classes, study sessions, and long hours of working on assignments. I would not have gotten to the point I am at without them, and am truly grateful for each person's friendship, as well as the memories that have come from this experience and Air Force assignment.

Joanna E. S. Williams

Table of Contents

Page

List of Figures

List of Tables

List of Abbreviations

CDDIS Crustal Dynamic Data Information System

CIS convective ionospheric storm

CLASS Comprehensive Large Array-Data Stewardship System

CORS Continuously Operating Reference Station

DoD Department of Defense

GLM Geostationary Lightning Mapper

GNSS Global Navigation Satellite System

GOES Geostationary Operational Environmental Satellite

GPS Global Positioning System

HF high frequency

HRAP Hydrologic Rainfall Analysis Projection

HURDAT HURricane DATabase

IPP ionospheric pierce point

LOS line of sight

MAPGPS MIT Automated Processing of GPS

MIT Massachusetts Institute of Technology

NAN not a number (as it pertains to Python code)

NASA National Aeronautics and Space Administration

NCAR National Center for Atmospheric Research

NCEP National Centers for Environmental Prediction

NESDIS National Environmental Satellite, Data, and Information Service

NHC National Hurricane Center

NOAA National Oceanic and Atmospheric Administration

NWS National Weather Service

RFC River Forecast Center

SST sea surface temperature

SWPC Space Weather Prediction Center

TC tropical cyclone

TEC Total Electron Content

TECU Total Electron Content Unit

TS thunderstorm

US United States

UTC Coordinated Universal Time

VTEC vertical total electron content

I. Introduction

Tropical cyclones (TCs) are large, natural, destructive phenomena causing significant damage to people, property, and resources. For example, Hurricane Michael (2018), is the 8th costliest hurricane in the United States (US) Atlantic basin to date with damages equating to 25 billion dollars (Beven II et al., 2019). Due to the high damage costs, it is important to prepare for the impacts of TCs. One method of preparing for and minimizing these impacts is through accurate forecasts of TCs, as they develop and intensify.

It is well known that the structure of the ionosphere is affected by several different sources, to include: solar radiation, geomagnetic activity, composition of the thermosphere, as well as energy transfer and wave activity from tropospheric weather (Sickle, 2018; Yu et al., 2015). Monitoring changes in total electron content (TEC) of the ionosphere is important to communications, positioning, navigation, broadcast, and financial systems. For example, Global Positioning System (GPS) signals can become impacted when there are significant changes in TEC, deteriorating the reliability and accuracy of position, navigation, and timing (PNT) for civilian and military applications (e.g., aviation, humanitarian aid, disaster relief) (National Coordination Office for Space-Based Positioning, Navigation, and Timing, 2006).

Currently, the influence of TCs on the structure of the ionosphere is an active area of research in the scientific community. By understanding the connection between TCs and the ionosphere, it might also be possible to develop a robust method for monitoring and forecasting TC intensification and movement. Previous studies have focused on how TCs and other tropospheric weather events cause gravity wave propagation in the ionosphere, altering the TEC. One study by Polyakova and Perevalova (2011) investigates the spatio-temporal TEC variations through observation irregularities in TEC through internal atmospheric gravity waves for three Category 5

hurricanes. This research implements comparisons between various TC parameters to localized TEC variation to isolate a TC as the primary cause of the changes in TEC during the occurrence of a TC, rather than through secondary effects caused by atmospheric or gravity waves.

Additionally, there are no widely known forecasting techniques for TCs involving TEC or GPS data. The objective of this research is to identify TEC variations and isolate the causes behind the variations. If accurate relationships can be identified between various TC parameters and TEC variations, then improved forecasting techniques, with the additional resource of near real-time TEC data, can be developed to track and forecast tropical cyclogensis and TC intensification. Furthermore, a motivation behind this research is: if there is an increased understanding behind TEC fluctuations, can it be identified that a single naturogenic and anthropogenic phenomenon is altering the ionosphere? This study begins with one of the largest naturogenic phenomenon, a TC; however, this process should be repeatable for other phenomena, such as thunderstorms, earthquakes, etc., as well as tracking anthropogenic events.

This chapter introduced the motivation and objective of this research while highlighting how this study is a new approach to a growing field of study. Chapter II provides a brief review on TCs, the atmospheric structure and the ionosphere, TEC, and some of the previous studies. Chapter III describes the methodology including the data selection, the Savitzky-Golay filter, how the data was processed, and the bootstrap method. Chapter IV presents the results of the TEC analysis, the relationship between the number of lightning flashes and the connection between rainfall rate to TEC variations. Lastly, Chapter V examines the potential impacts of this research, some of the limitations, and proposed future work ideas.

II. Background

2.1 Tropical Cyclones

TCs are warm-cored, cyclonic, low pressure systems that form over warm tropical oceans and vary in size, intensity, and structure (Chan and Kepert, 2010). There are six conditions generally associated with TC development, or tropical cyclogenesis: sea surface temperatures (SST) greater than 26.5°C in the uppermost 50 m of the ocean's mixed layer, a moist mid-troposphere, cooling temperatures with height that are significant enough for the atmosphere to be potentially unstable due to moist convection, a location where Coriolis effects are apparent (i.e. at least 300 miles away from the Equator), pre-existing near surface disturbance, and minimal vertical wind shear (Landsea, 2014; Shultz et al., 2005).

Determination of TC stages are established by the maximum wind speed and minimum surface pressure within the eye of the storm. TCs begin as areas of enhanced convection called tropical disturbances. If the area of enhanced convection develops a rotational circulation, it can enter either or both TC stages——tropical depression with maximum sustained surface winds of less than or equal 33 kts, and tropical storm with maximum sustained surface winds ranging from greater than 33 kts to less than 64 kts. Systems that are tropical depressions are numbered, and those that reach tropical storm category thresholds are named. When there is enough energy and moisture, the low pressure system can intensify into a typhoon (Pacific), cyclone (Southern Hemisphere), or hurricane (Atlantic). The Saffir-Simpson Scale (Atlantic) categorizes hurricanes with maximum sustained surface winds greater than or equal to 64 kts (Table 1) (Shultz et al., 2005).

There are three main components to the TC structure. In the center, there is a relatively calm region known as the eye. The eye typically has a diameter that

Table 1. The Saffir-Simpson Hurricane Wind Scale categorizes TCs in the Atlantic Ocean.

Category	Wind Speed (kt)
1	64-82
2	83-95
3	96-112
4	113-136
5	137 or higher

ranges between 20 and 100 km. Surrounding the eye, is the eye wall, which contains the strongest rotation and winds (Chan and Kepert, 2010). Next, rainbands are elongated areas of precipitation, which can be convective or stratiform in nature, that spiral outward from the center of a TC. The inner rainbands are located from just outside the eye wall out to 80-120 km from the center of the storm, with the position of these rainbands being dependent on the TC structure and direction of travel. The outer rainbands occur typically between 120-150 km from the center of the TC, but can stretch even beyond 300 km (Molinari et al., 1994).

2.1.1 Lightning and Convection in Tropical Cyclones

Lightning within a TC has a radial distribution in a mature hurricane, with the lightning density varying in each of the three regions of a TC: the eye wall, inner rainbands, and outer rainbands. In a study on Hurricane Andrew (1992), Molinari et al. (1994) found a relationship between lightning occurrence, the eye wall structure, and the intensity variation.

The eye wall in a TC typically has the highest cloud tops and a weak cellular structure due to the high, cold cloud tops, which limits the amount of liquid precipitation above the freezing level, creating an efficient transport of ice in a hurricane, both downward and horizontally. These motions and features disrupt the TC structure from having the necessary conditions for stronger convective activity in the eye wall. A period when intense convection may be more likely in the eye wall is during an

eye wall replacement cycle. This is when an outer eye wall develops and continues to evolve, limiting the resources for the inner eye wall to sustain its strength, and thus the outer eye wall eventually replaces the inner eye wall as the main center structure of the storm (Molinari et al., 1994).

The region of the inner rainbands can contain strong convection; however, typically they are not highly cellular. In comparison, the outer rainbands extend further from the warm-core center structure of the TC, and they exist in an environment that closely resembles the tropical or subtropical atmosphere around the storm itself. The surrounding atmosphere has greater instability. Additionally, the rotation dynamics of a TC contribute to a more convective structure in the outer rainbands. In the eye wall, the rotation is much stronger and contains higher speeds than in the outer rainbands. The weaker rotation allows convection to vary rapidly and contain the strong updrafts and cold downdrafts needed for convection. These features identify the outer rainbands to be the most convective in nature of the three structural distributions for a TC (Molinari et al., 1994).

Within 300 km of the eye, Molinari et al. (1994) found that the number of flashes per 100 square kilometers per day was nearly zero for 40-100 km from the center of the storm, and reached a peak in the 180-200 km range. Additionally, the greatest concentration of lightning flashes was found in the northeast quadrant and to the right of the storm motion for majority of the studied period.

2.1.2 Precipitation in Tropical Cyclones

The components of TC formation are also factors in TC precipitation distribution and intensity, to include the environmental components (e.g. wind shear, SST, moisture distribution) and dynamic components (e.g. intensity, location, track, and speed of the TC) (Lonfat et al., 2004). There are two types of precipitation found

in a TC: convective and stratiform rain. Areas of convective precipitation are where the updrafts are more intense, and are the most likely to produce lightning. Additionally, convective precipitation is typically shorter lived. In comparison, stratiform precipitation takes place in a relatively stable environment and lasts for longer times frames with a more consistent rainfall rate (Lonfat et al., 2004; Molinari et al., 1994).

Similar to the lightning distribution in a TC, precipitation can also be categorized within the three structural sections of a TC. First within the eye wall, there is typically a ring of intense precipitation associated with the high speed rotation. According to Lonfat et al. (2004), the heaviest rain is located between 35-60 km from the storm center. The location of the strongest precipitation relative to the radius from the center of the storm decreases with increasing TC intensity (Lonfat et al., 2004).

Next, the inner rainbands contain more stratiform precipitation and they are areas which on weather radar may appear as bright bands. These regions are significant since they can extend more than 100 km from the eye, and are areas of suppressed convection. Also, the inner rainbands contain the stratiform rain that can account for more than half the precipitation within 100 km of the center, and can be categorized as covering 10 times the area of convective rain (Molinari et al., 1994). Lastly, the outer rainbands contain more convection and appear to have less intense rainfall rates. According to Lonfat et al. (2004), the greater the radial distance from the TC center, the lower the mean rainfall rate in general, with only occasional relative maximum peaks (within 100 km) in rainfall rate. One reason the mean rainfall rate is lower for the outer rainbands is because most of the area between these rainbands is free of precipitation.

2.2 Ionosphere

The Earth's atmosphere is composed of five primary layers: the troposphere, stratosphere, mesosphere, thermosphere, and exosphere (Figure 1). The troposphere is the lowest part of the atmosphere extending from the surface to approximately 10 km in altitude. This layer is where the majority of terrestrial weather, including TCs, occur. The ionosphere extends from the mesosphere (approximately 50 km in altitude) into the exosphere (beginning at 500 km and extending to approximately 10,000 km). This layer is composed of plasma with positively charged ions and negatively charged electrons (Sickle, 2018).

Changes in electron density may cause transmitted radio signals to fluctuate significantly in amplitude and phase, in a phenomenon referred to as "ionospheric scintillation" (Ke et al., 2019). The magnitude of scintillation depends on six factors: geographic location, local time, season, geomagnetic activity, solar cycle, and waves from the lower atmosphere that propagate into the ionosphere (Space Weather Prediction Center, 2019a). During the daytime, there are four regions that make up the ionosphere: D, E, F1, and F2, with D being closest to the Earth. During the night, the primary persisting layer is the F2 region. This region is the densest section of the ionosphere "responsible for most sky wave propagation of radio waves, facilitating high frequency (HF) radio communications over long distances" (El-naggar, 2011). Figure 7.1 in Tascione (2010) depicts the diurnal changes in electron density for the layers of the ionosphere during solar minimum and maximum. The electron densities increase daily during the daytime and decrease by one or two orders of magnitude at night. Additionally, the electron densities are lower during times of sunspots and solar minimum (Tascione, 2010).

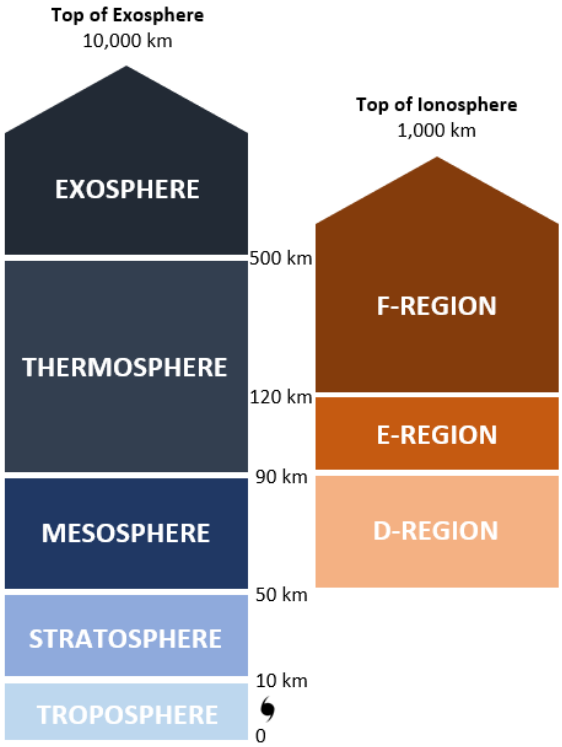

Figure 1. On the left hand side are the layers of the atmosphere with the approximate altitudes at which each layer begins annotated. On the right side, the corresponding heights for the layers of the ionosphere are shown, stretching from the mesosphere into the exosphere.

2.2.1 Total Electron Content

According to Hegarty and Chatre (2008), ionospheric scintillation can be quantified through measurements of Total Electron Content (TEC) fluctuations. TEC is derived from dual-frequency Global Navigation Satellite System (GNSS) data and is defined as the total number of electrons per square meter along a path between a radio transmitter and GNSS receiver, where 1 TEC Unit (TECU) is equal to 10^{16} electrons per square meter. Currently, there are six operational GNSS constellations: GPS (United States; 24 satellites), Globalnaya Navigazionnaya Sputnikovaya Sistema (GLONASS; Russian; 24 satellites), Galileo (Europe; 26 satellites), BeiDou (China; 33 satellites), Quazi-Zenith Satellite System (QZSS; Japan; 4 satellites), and Indian Regional Navigation Satellite System (IRNSS; India; 7 satellites) (Hegarty and Cha-

tre, 2008; National Coordination Office for Space-Based Positioning, Navigation, and Timing, 2017).

The combination of GNSS satellites, ground stations, and GNSS receivers provides position, navigation, and timing (PNT) information. A receiver needs to have direct line of sight to four satellites in order to calculate four unique quantities: latitude, longitude, altitude, and time, where time is in Coordinated Universal Time (UTC) (Government Office for Science, 2018).

GNSS satellites transmit radio signals at two main frequencies: the L_1 band at 1575.42 MHz (f_1) and the L_2 band at 1227.60 MHz (f_2) (Government Office for Science, 2018). The L_1 and L_2 frequencies can be used to calculate TEC using the following equation:

$$TEC = \frac{c}{40.3}(\frac{1}{f_1^2} - \frac{1}{f_2^2})\delta_{\tau_{f_f f_2}} \tag{1}$$

where c is the speed of light (in m/s), and $\tau_{f_f f_2}$ is the difference of travel time between both radio signals (El-naggar, 2011). A dual-frequency receiver can model and remove a significant portion of the bias (satellite and receiver), as well as removing the effects of the neutral atmosphere, resulting from TEC calculations. In particular, the higher the frequency employed, the smaller the delay in travel times between satellite and receiver (Sickle, 2018).

2.2.2 Radio Signals in the Ionosphere

There are four primary effects on radio signals traveling from a satellite to a GNSS receiver: (1) passes through the ionosphere, uninhibited, (2) reflects off the ionosphere, (3) refracts in the ionosphere, or (4) is otherwise delayed in the signal transmission, as compared to the speed of light in a vacuum (Sickle, 2018; Space Weather Prediction Center, 2019b). Because the ionosphere is dispersive in nature to radio frequencies—meaning the angular frequency (ω) and wave number (k) are not

linearly-proportional to each other—the resulting travel time of a radio signal from a satellite to a GNSS receiver is heavily dependent on the TEC composition of the ionosphere and the signal frequency. In other words, the result is that the refractive index is dependent on the radio frequencies employed (i.e. L_1 versus L_2, or L_1 and L_2).

$$\omega^2 = c^2k^2 + \omega_p^2 \tag{2}$$

$$\omega_p = 2\pi f_p \text{ with } f_p = 8.98\sqrt{N_e} \text{ (in Hz)}, \tag{3}$$

where ω_p is the critical frequency of the ionospheric plasma, $f_p \simeq 10^6$-10^7 Hz, and N_e is the electron density (in electrons per cubic meter) (Subirana et al., 2011). When $\omega < \omega_p$, the signal will be reflected, while if $\omega > \omega_p$, the signal will pass through the ionosphere. Additional details on the angular frequency, wave number, the phase refractive index, ionospheric delay, and deriving TEC are provided in El-naggar (2011) and Subirana et al. (2011).

2.3 Previous Research

Many studies have found evidence that tropospheric weather causes impacts to the ionosphere. One theory is that the energy from the lower part of the atmosphere is carried to the ionosphere through atmospheric tides—large-scale waves that are generated by tropospheric weather and propagate upward (Immel et al., 2009). According to Immel et al. (2009), atmospheric tides were previously thought to dissipate at the base of the ionosphere; however, further studies have identified that the upper ionosphere is impacted with the complex dynamic forcing of the atmospheric tides. The variability seen in the ionosphere causes instability, sometimes known as convective ionospheric storms (CIS). These CISs are similar to ionospheric scintillation (ref. Section 2.2), where the instability in the ionosphere causes density irregularities af-

fecting the radio wave propagation, GNSS signals, or navigation failure (Immel et al., 2009). Additional studies exploring the relationship between tropospheric weather and the variability in the ionosphere include: Huang et al. (2019) and Isaev et al. (2010).

2.3.1 Total Electron Content Variation Over Thunderstorms

Lay et al. (2013) explored how TEC fluctuated over the US Great Plains for three large thunderstorm (TS) nights and one small TS night—characterized by a maximum lightning density of 0.5 km^{-2}. They calculated vertical TEC (VTEC) values from the slant TEC—i.e. "integrated electron densities along a line of sight from satellite to receiver"—which was derived from GPS receivers from the L_1 and L_2 signals (Lay et al., 2013). The data was detrended using a 6th order polynomial by subtracting out the best fit polynomial, allowing the data used to be only sensitive to higher-frequency variations. In this study, the lightning was used as a proxy for the intensity of the TS, based on the maximum lightning density and the peak lightning rate. The small TS night showed little variation when compared to the large TS nights. The large TS nights showed larger TEC variations, with maximum peak-to-peak variation of approximately 1.4 TECU. Additionally, for these thunderstorms, the lightning was clustered to the east and north or the west and north of the storm depending on the day and which satellite was used as the reference point for comparison. Furthermore, when compared to the results of additional satellites, with lower maximum elevation angles, the TEC variations were visible for the large thunderstorm nights, although they were not as pronounced. This is potentially due to the longer slant path from the satellite to the receiver. They found that with significant TS activity there was more high-frequency content than typical background TEC fluctuations; however, they were not able to conclude with confidence which

mechanism was responsible for the perturbations (Lay et al., 2013).

2.3.2 Tropical Cyclone Effects on Total Electron Content

Some studies have not been able to develop conclusive relationships between TCs and TEC primarily because it is difficult to separate the disturbances associated with a TC; however, Polyakova and Perevalova (2013) were able to make this distinction when using data during quiet geomagnetic conditions. They looked at how TCs cause TEC disturbances related to the intensity and location of the TC for the time delay of effects and magnitude of the disturbances. Their research focused on TCs in the North-West Pacific Ocean, or typhoons, using ground-based, double-frequency GPS receivers. The line of sight (LOS) and ionospheric pierce point (IPP)—the location at which the GPS signal crosses the threshold of the ionosphere—were used with relation to GPS receiver locations to estimate the spatial localization of the TEC disturbances. They studied 24 typhoons and found that TEC increased and the greatest TEC variations were observed when the TCs were most intense, with the fastest wind speeds, and at low elevation angles for the LOS. One typhoon had approximately 5 TECU increase relative to monthly averages upon landfall (Polyakova and Perevalova, 2013).

Polyakova and Perevalova (2011), investigated Hurricanes Katrina (2005), Rita (2005), and Wilma (2005) with regard to spatio-temporal TEC variations through dual frequency ground-based GPS receivers and National Centers for Environmental Prediction (NCEP)/National Center for Atmospheric Research (NCAR) Reanalysis data. In this study, they condcuted their investigation for time periods during quiet geomagnetic activity and local evening/nighttime to minimize the background TEC variability. Through all three cases, Polyakova and Perevalova (2011) found irregularities in the ionospheric plasma over the TC trajectories through internal atmospheric

waves. Additionally, the longer the period of variation observed, the greater the TEC variation amplitude, and the larger the area covered by atmospheric waves (Polyakova and Perevalova, 2011).

In contrast, Guha et al. (2016) found that TEC decreased for TCs making landfall, and TEC depleted further during the day following landfall. They analyzed TEC values from GPS satellites and a multitude of GPS receivers, converted slant TEC to VTEC using a mapping function for different ionospheric pierce points, and compared the VTEC to the monthly mean for multiple TCs in the Indian sector, specifically the Bay of Bengal. TCs are extended, long lasting disturbances, hence they believe the decrease in VTEC is experienced the day the TC makes landfall, and prolongs into the following day with a further decrease. Due to the number of charged particles decreasing in the ionosphere as a TC approaches land, there is a decrease in the VTEC compared to the monthly mean. As chemical constituents are redistributed in the ionosphere, the number of neutral particles through the ionosphere increases, resulting in a decrease in TEC over the path of measurement. Furthermore, there are changes in the chemical composition of the ionosphere as a TC makes landfall. One limitation of this study is that GPS receivers in the area may not have accurately represented the TC environment in all directions (Guha et al., 2016).

III. Methodology

3.1 Data Selection

There are four data sets used in this study: hurricane, total electron content, lightning, and precipitation. The hurricane data is used as the reference point for the location of the TC to determine localized effects. TEC data is used to characterize the state of the ionosphere above the studied TC. The lightning and precipitation data are used as proxies for the electric and dynamic components of a TC.

3.1.1 Hurricane Data

The National Hurricane Center (NHC) collects all available hurricane observations, conducts a post-storm analysis of each TC, and creates the HURricane DATabase (HURDAT) files with the best track information for each storm (Landsea et al., 2015). HURDAT information includes: TC name, date, UTC time, record indicator (e.g. landfall, maximum sustained wind speed, minimum central pressure, etc.), TC status, latitude and longitude position, maximum sustained winds (in knots), minimum pressure (in millibars), and a variety of wind radii maxima extending in the quadrants surrounding the center of the TC (Landsea et al., 2015). In 2013, HURDAT2 (the second generation of HURDAT) came online with additional data such as landfall and intensity maxima, in addition to the standard synoptic report times of 00, 06, 12, and 18 UTC, non-developing tropical depressions, and best track wind radii. This anlysis uses the date, time, latitude, and longitude directly from the HURDAT2 file and additional information on Hurricane Michael (2018) from Beven II et al. (2019), to include the total storm rainfall analysis.

3.1.2 Total Electron Content Data

TEC data was accessed from the MIT Haystack Observatory Madrigal database (Coster, 2019). Each file contains five variables: timestamp, latitude, longitude, TEC (TEC), and dTEC (TEC error). The data has a global grid spacing of 1° latitude by 1° longitude at 5-minute intervals (time steps) over a 24-hour period. The TEC value at each grid point is the median of all TEC measurements within a 1° latitude by 1° longitude area during the 5-minute period (Rideout and Coster, 2006). This data set was created using data from all available GNSS satellites and processed through the MIT Automated Processing of GPS (MAPGPS). No underlying models smoothed out gradients within the processed data. MAPGPS is designed with three goals: (1) "to compute absolute values of TEC, along with their associated error bars, worldwide," (2) "to produce a scalable algorithm, i.e., software that is able to process each day independently, without requiring any previous days' results," and (3) "to select the best mapping function to process the data ... to convert line of sight TEC to zenith TEC" (Rideout and Coster, 2006).

A mapping function is used to convert LOS, or slant, TEC to VTEC. The mapping function is defined by:

$$z = \frac{1}{\sqrt{(1.0 - (F\cos(el)^2))}} \tag{4}$$

where F is the fit parameter and el is the elevation angle. A value of 0.95 is used for F in MAPGPS as it is found to best minimize the value of the figure of merit, with an elevation angle cutoff of 7°, and an IPP of 450 km (Rideout and Coster, 2006).

During the processing of the data, satellite and receiver biases are calculated and accounted for in the final product of the TEC values, as both hardware contribute delays between the L_1 and L_2 signals. These delays are important calculations in

that their removal from the raw data helps to represent the ionosphere accurately. For reference, "1 TECU is equivalent to a delay in units of distance of 0.163 m at the L_1 frequency and 1 TECU is also equal to a delay in time for the L_1 signal of 0.54 ns." Since the satellite biases have been found to be relatively constant, the estimated values from the Crustal Dynamic Data Information System (CDDIS) are used in MAPGPS (Rideout and Coster, 2006).

The receiver biases vary more than the satellite biases; therefore, the data undergoes a combination of three techniques: minimum scalloping, least squares, and the zero TEC method. First, the minimum scalloping technique accounts for the fact that the zenith TEC values computed from low elevation angles should be similar to those from high elevation angles. This technique is applied at local midnight and is averaged over relatively longer time periods to minimize the ionospheric diurnal effects in the calculations, to get a result of the flattest value of TEC versus elevation angle. Next, the least squares method only provides relative biases, not the absolute value of biases. This method uses a system of equations focused on the differential relationship between the different receiver biases. Lastly, in the zero TEC method, the minimum observed TEC value within a 24-hour period is set to zero, since TEC is often close to zero during the night or at high latitudes. More information on these techniques are described in Rideout and Coster (2006).

3.1.3 Lightning Data

The lightning data used in this study is the Geostationary Lightning Mapper (GLM) data from the Geostationary Operational Environmental Satellite (GOES) –16 satellite, positioned at 75.2°W, at an altitude of 36,000 km, with an inclination angle of 0°. This satellite provides a view centered on the Americas and a near uniform spatial resolution ranging from 8 to 14 km and covering latitudes from 52°N

to 52°S (Goodman et al., 2012a). GLM is a single-channel, near-infrared detector that operates at a wavelength of 777.4 nm, detecting lightning day and night through an electronic scanning technique, with three mission objectives: "(1) provide continuous, full disk lightning measurement for storm warning and nowcasting, (2) provide an early warning of tornadic activity, and (3) accumulate a long-term database to track decadal changes of lightning" (Goodman et al., 2012a). GLM has a frame rate of 2 milliseconds, a product latency of 20 seconds, and a download data rate of 7.7 megabits per second, allowing forecasters to utilize nearly real-time data to adjust their forecasts (Goodman et al., 2012a).

GLM data from the National Oceanic and Atmospheric Administration (NOAA) is accessible through the NOAA Comprehensive Large Array-Data Stewardship System (2019) (CLASS). The first iteration of GLM data starts with GOES–16, beginning in March 2017. The satellite and data files are formatted at 20-second intervals and contain three base products: events, groups, and flashes. An event is the occurrence of a lightning pulse in a single pixel exceeding the background threshold during a single time frame and it is considered the basic unit of data from GLM. A group is when there are multiple events adjacent to each other (i.e. a single lightning discharge illuminated more than one pixel during a single time frame). In comparison to an event and a group, a flash consists of one or more optical pulses within a specified time and distance (Goodman et al., 2012a). Figure 2 shows the flowchart for how GLM determines how to process different lightning occurrences (Goodman et al., 2012b).

Numerous calculations are conducted pixel by pixel to determine the radiance and energy of a lightning pulse. These determined values, along with latitude, longitude, the time of the occurrence, the energy, and the area of the pulse, help classify the pulses into the three base products and derive 48 parameters. Figure 3 shows an example of how the data is processed for an event, group, and flash (Goodman et al.,

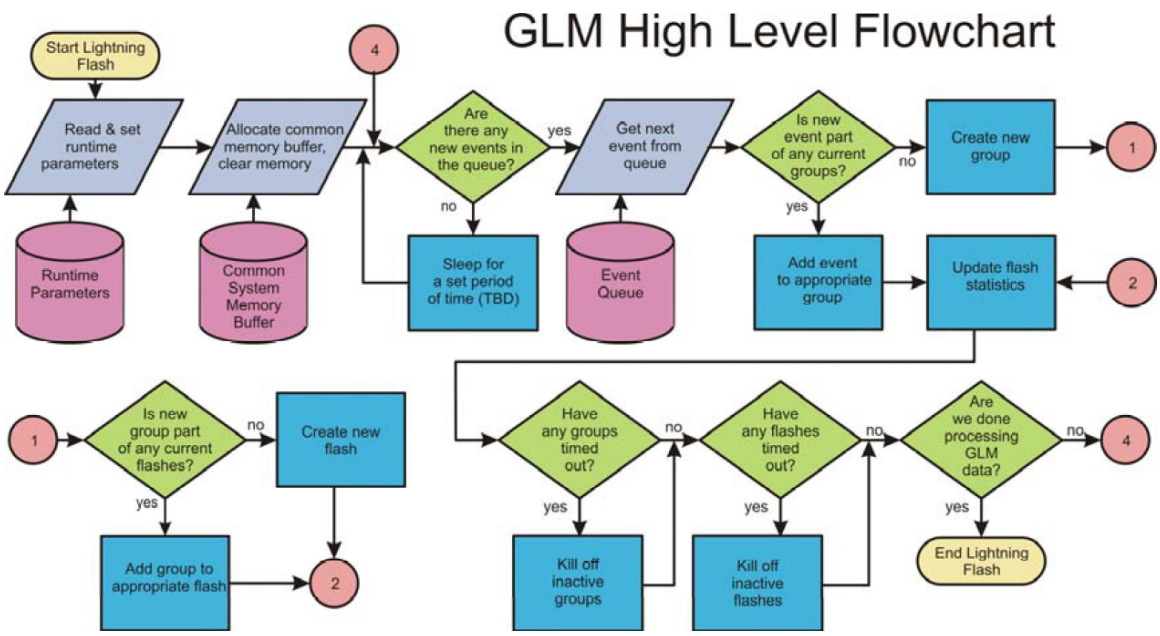

Figure 2. GLM flowchart displaying the process the geostationary lightning mapper undergoes to differentiate lightning occurrences between an event, a group, and a flash. Courtesy of NASA and NOAA (Goodman et al., 2012b).

2012b). The data is processed through the Lightning GLM Cluster Filter Algorithm (LCFA) by utilizing the 48 parameters to place and determine whether the event, represented by each individual numbered box in Figure 3, data fits into a group, represented by more than one box of the same color, or the bold border of a box identifying more than one event in that box (e.g. events 11 and 12). From there, a group or multiple groups are placed into a flash, represented by the clusters of events and groups, based on time and distance criteria. Figure 3 shows 12 events, six groups, and two flashes. Additional details can be found in the Algorithm Theoretical Basis Document by Goodman et al. (2012a).

3.1.4 Precipitation Data

The Environmental Modeling Center (EMC) from NCEP produces the Stage IV precipitation data used in this study. Both Stage II and Stage IV data are hourly and 6-hourly, 4-kilometer analyses. The Stage II data is produced from real-time gauge

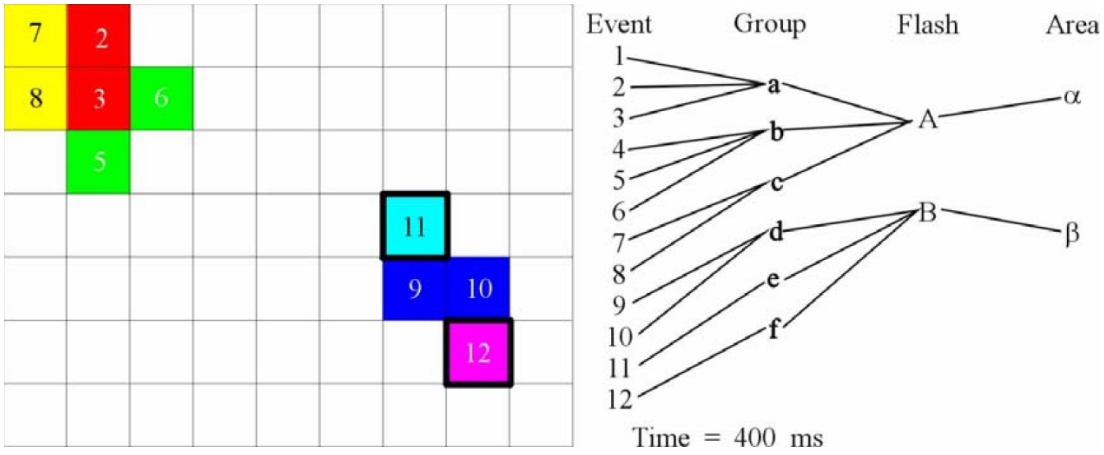

Figure 3. GLM example of differentiating a lightning event, group, and flash. Events are represented by each individual numbered box, groups are represented by more than one box being the same color, or the bold border of a box identifying more than one event in that box (e.g. events 11 and 12), and flashes are represented by the clusters of events and groups, based on time and distance criteria. Courtesy of NASA and NOAA (Goodman et al., 2012b).

and WSR-88D radar data, consisting of no manual quality control. The Stage IV data is developed from Stage II data from NCEP based on regional multi-sensor analyses completed by National Weather Service (NWS) River Forecast Centers (RFC). Figure 4 demonstrates a mosaic of the regional analyses (Lin and Mitchell, 2005).

The Stage IV processing consists of the RFC generating each hourly and 6-hourly analysis twice. The first analysis is an automated one with no manual quality control, and is completed after the end of the accumulation time period. Several hours later, the second analysis is completed in a manual mode with a human analyst completing a quality control check of the information. Next, the mosaic is created at 35 minutes after the top of each hour; however, the mosaics continue to get updated as more data is received by the RFCs, with a relatively finalized product for the hourly mosaic being completed approximately 12-18 hours later (Lin and Mitchell, 2005).

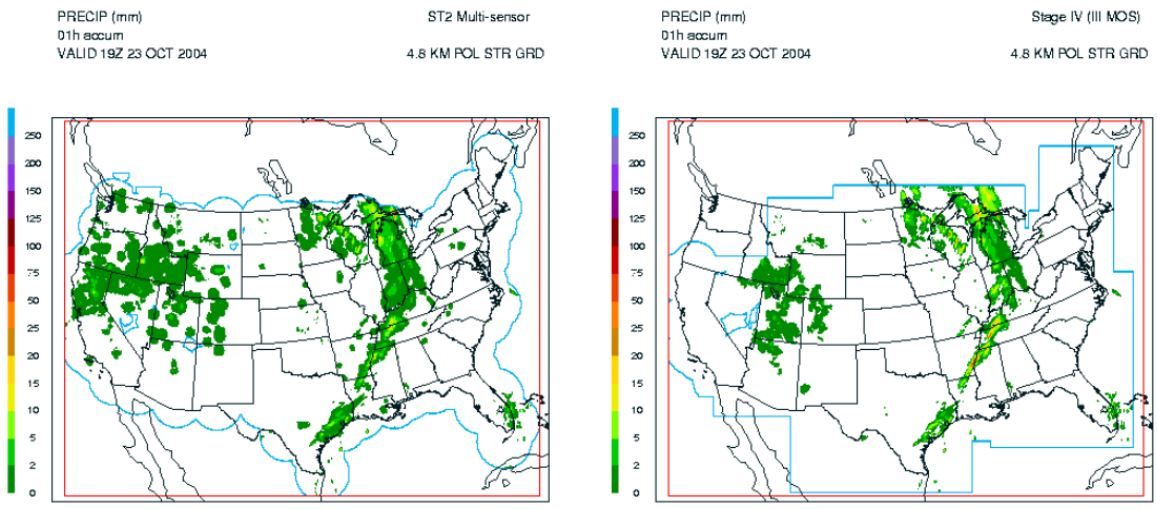

Figure 4. "Snapshot of a one-hour Stage II (left) and Stage IV (right) analysis." Courtesy of NCEP/EMC (Lin and Mitchell, 2005).

3.2 Savitzky-Golay Filter

The Savitzky-Golay filter uses a moving polynomial and the method of least-squares to smooth out data (Savitzky and Golay, 1964). This method is used when the data is slowly varying, or corrupted by noise. It uses a moving window with a set number of points. For each point's center point of the window, a new least-squares fit at the designated polynomial is calculated, rather than being influenced by the surrounding points' calculations. The Savitzky-Golay filter is most useful with larger data sets to allow for more smoothing (Press and Teukolsky, 1990). Additionally, a higher order polynomial is able to preserve the widths and heights of a varying curve, if it is not consistent throughout the data (Press and Teukolsky, 1990).

In this case study, the noise removed from the TEC data was the diurnal cycle to be able to better identify fluctuations or deviations in the TEC values. Finding the right balance of smoothing was explored through varying the window size and the order polynomial for the best fit. Figure 5 demonstrates the variations of how the different windows and ordered polynomials fit the data for 30°N, 86°W, one of the positions of Hurricane Michael. Since the TEC data naturally experiences a diurnal

cycle, the goal of the best fit curve was to demonstrate the diurnal cycle without tracking the deviations too closely. The less the window time, the more the Savitzky-Golay filter line followed the shape of the peaks, to include the smaller ones. If the line followed the smaller peaks too closely, then the atypical variations got lost in the best fit line.

In Figure 5, on 10 October there were more peaks than on 11 or 12 October; hence, it is desirable to keep those peaks highlighted as greater variations, rather than as "normal." Then, in comparison, the seven-hour window was very similar to the six-hour window; therefore, it was beneficial to include the 12 data points from the additional hour for extra calculations. In the end, for this study, the Savitzky-Golay filter used a six-hour window and 3rd order polynomial. The six-hour window followed the shape of the data in general, creating a best fit curve. The 3rd order polynomial was a happy middle ground that follows the boarder shape of the TEC data points, where the 1st order did not take enough points into account for the purpose of the study, and the 5th order followed too many points.

The change in TEC (ΔTEC) used in the calculations for this study were the values of the Savitzky-Golay filter applied to each time. Additionally, the absolute value of the change in TEC ($|\Delta TEC|$) was taken to look at the positive values and the magnitude of the fluctuations in TEC.

3.3 Research Overview

Hurricane Michael (2018) is an ideal case study based on its end strength, intensification, and its close proximity to continuously operating reference station (CORS) receivers (Figure 6) (National Geodetic Survey, 2019). Its end strength of Category 5 and its rapid intensification to this strength within 24 hours provides the signatures needed to identify how a TC influences the ionosphere, in an extreme case.

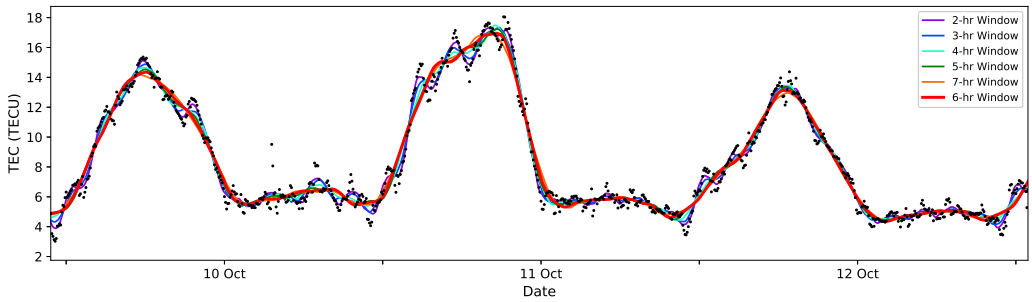

(a) Varying window size

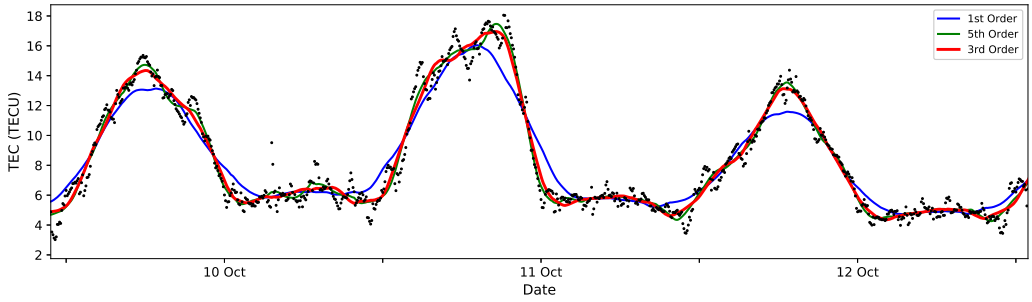

(b) Varying order of polynomial

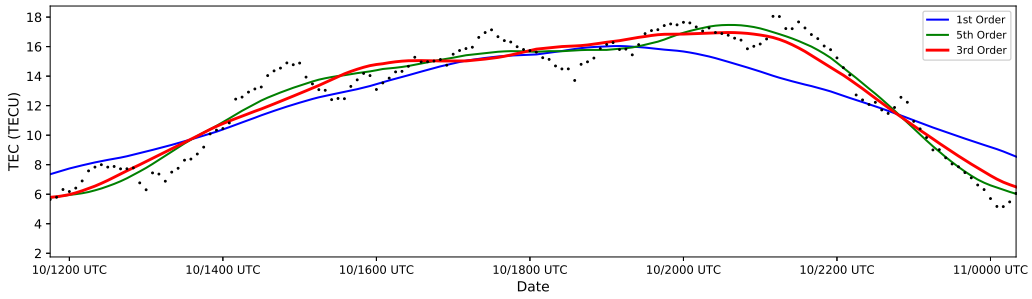

(c) Varying window size zoomed in on 10 October

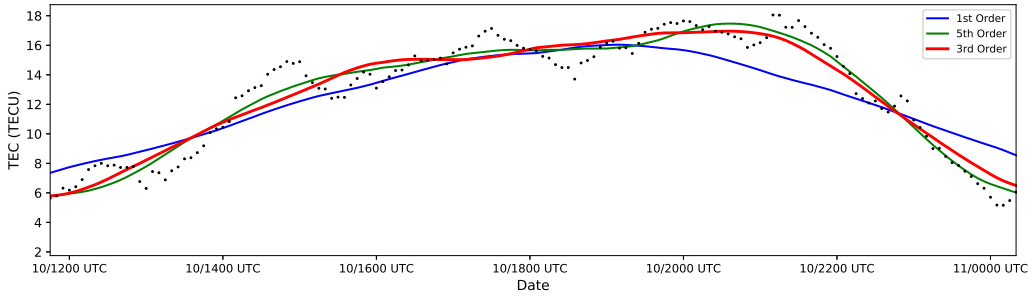

(d) Varying order of polynomial zoomed in on 10 October

Figure 5. Using the Savitzky-Golay filter, the window spread for the TEC data trying to find the best fit of a diurnal curve without following the data points too closely. The black dots are the raw data points for 30°N, 86°W, one of Hurricane Michael's recorded locations. (a) The variation of different window sizes, with a 3rd order polynomial. (b) The variation of the order polynomial with a six-hour window. (c) A zoomed in view of the varied window size for 10 October from 12 UTC through 00 UTC on 11 October. (d) A zoomed in view of the varied ordered polynomial for 10 October from 12 UTC through 00 UTC on 11 October.

Hurricane Michael formed on 6 October and became a tropical depression on the morning of 7 October in the Caribbean Sea, east of Belize. Later on 7 October, the TC reached tropical storm strength, and within 24 hours, on 8 October it reached hurricane strength. During these 30 hours, the TC progressed northeast toward the western edge of Cuba. In the following 48 hours, Hurricane Michael continued to strengthen from a Category 1 storm to reaching Category 4 strength during the morning of 10 October. On 10 October 2018, Hurricane Michael reached maximum intensity and made landfall along the Gulf Coast of Florida (Figure 7), providing five TC location data points, rather than four on the other days of the TC (Beven II et al., 2019). These five points are annotated in red in Figure 8. Additionally, all four types of data were available for the time period of Hurricane Michael. The lightning data was a limiting factor for analyzing a different TC, since GLM has only been reporting since March 2017.

3.4 Data Processing

Each type of data varies in temporal resolution and area of coverage. The TEC data has one value for each 1° latitude by 1° longitude box, and determined the spatial resolution. Additionally, since the data comparison was to TEC, the five-minute interval with 288 data points per day was used for the temporal resolution. The five points for the location of Hurricane Michael's eye on 10 October 2018, from the best track data, were used as reference points in the calculations for this study.

3.4.1 Reformatting the Data

The area of focus for this study is the Gulf of Mexico and Florida coastal area, marked by the green square in Figure 8. The range of latitudes used are 22°N to 34°N and 78°W to 90°W for longitudes. These latitudes and longitudes were chosen because

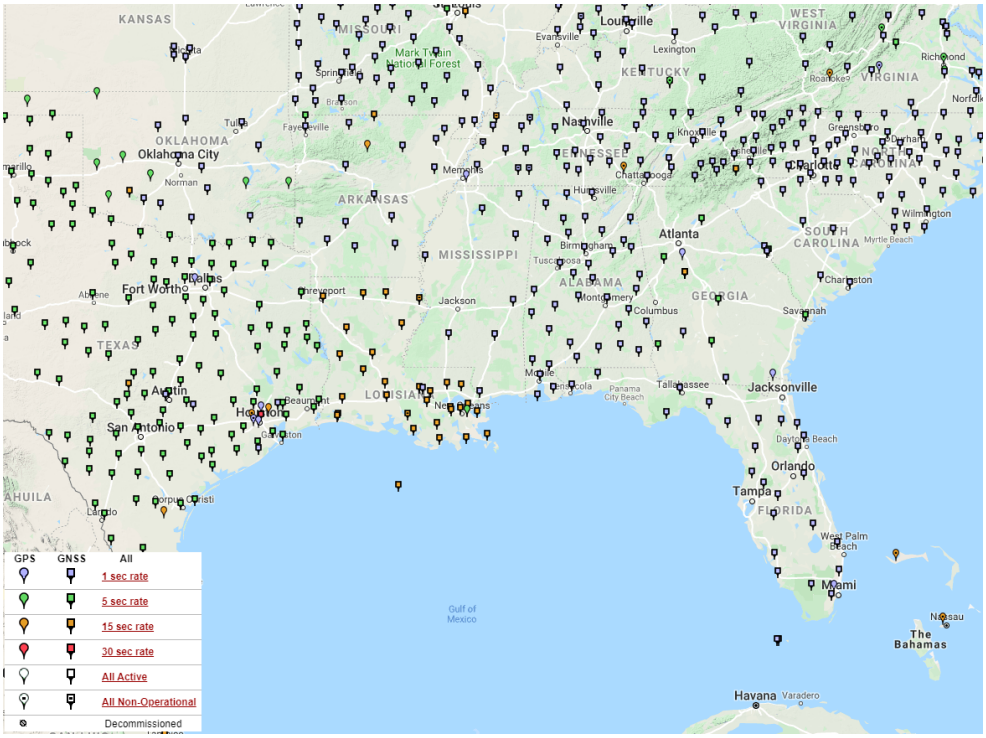

Figure 6. Display of all the CORS for GPS and GNSS receivers for the Southeastern United States and Gulf of Mexico region. Courtesy of NOAA/NGS (National Geodetic Survey, 2019).

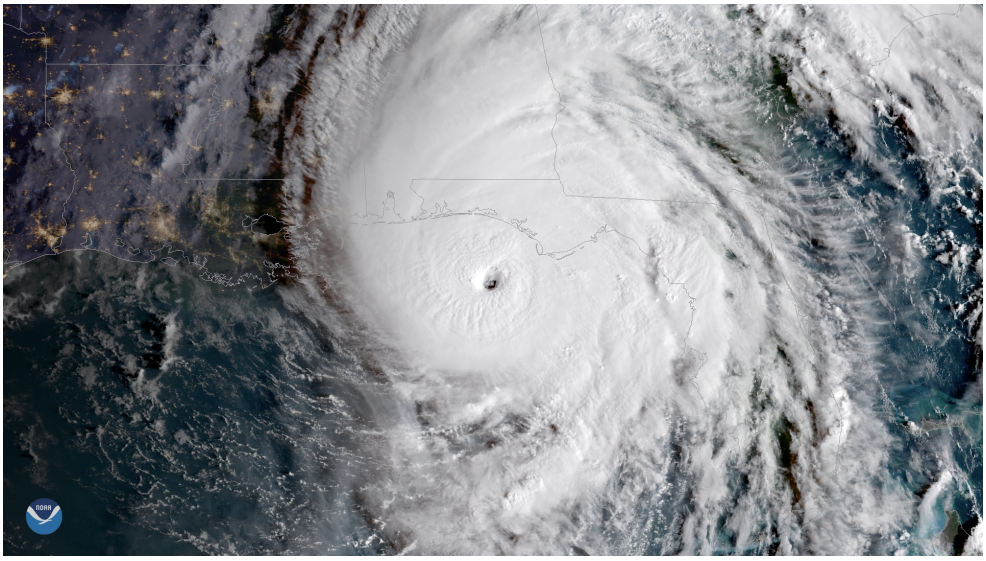

Figure 7. Satellite image of Hurricane Michael on 10 October 2018. Courtesy of NOAA/NESDIS (Leslie and Bateman, 2018).

they encompass the area of Hurricane Michael, mainly on 10 October; however, this area also allowed for investigation of the rainbands extending outward from the eye of the storm. Each data set was isolated to cover this 12° by 12° area.

The lightning and precipitation data were reformatted into arrays to match the size of the daily TEC data files over the Gulf of Mexico with 288 time steps, 12° of latitude, and 12° of longitude. The GLM data was compiled for each five-minute interval to contain fifteen 20-second lightning files, and the number of lightning flashes occurring during a given five-minute period for each 1° by 1° box were counted.

The precipitation data was produced on the national Hydrologic Rainfall Analysis Projection (HRAP) grid, which is a polar stereographic grid. The data was processed using a kd-tree to match up this data to the TEC data grid (Lin and Mitchell, 2005). The kd-tree is a method using the nearest neighbor to determine the corresponding approximate value (Greenspan and Yurick, 2003). Since the HRAP grid contains two-dimensional arrays for both latitude and longitude, the kd-tree method uses approximations to result in a two-dimensional array containing both latitude and longitude as the two components of the array, rather than as separate arrays. Through this method, the precipitation data was reformatted to a 1° by 1° grid and then could be isolated to the designated 12° by 12° box described above. In addition, the precipitation data was hourly, therefore, to create an array with 288 time steps to match the TEC data, each hour's rainfall rate was repeated for the 12 five-minute intervals within an hour.

3.4.2 Binning the Data

This study aims to find a correlation between the absolute value of the change in TEC ($|\Delta TEC|$) and the number of lightning flashes, as well as varying the rainfall rate in a TC. The analysis examines (1) the closest eight 1° by 1° boxes surrounding

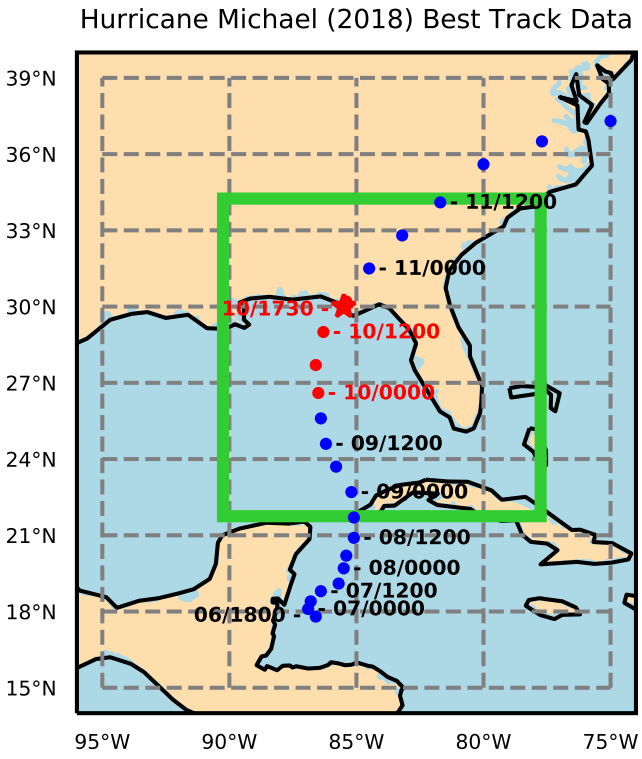

Figure 8. NHC best track data for Hurricane Michael (2018). The data points in red are annotating the positions of Hurricane Michael on 10 October 2018. The green square outlines the latitudes and longitudes used in this study.

the eye of the TC (shown in red in Figure 9) and (2) the 16 boxes 2° out from the TC center (shown in blue in Figure 9). Each 1° of latitude by 1° of longitude box is approximately 110 by 90 kilometers, and includes the eye wall and inner rainbands. The boxes 2° away from the TC center cover the majority of the outer rainbands, as in Molinari et al. (1994). The five TC locations from the NHC best track data were used for each of the calculations. For the upcoming figures, the red and blue lines are composed of the data surrounding each of the TC center points, resulting in forty-five 1° by 1° boxes for the red lines and eighty 1° by 1° boxes for the blue lines.

The lightning data was binned into 11 categories for lightning flashes zero through nine, and one final category for greater than nine lightning flashes.The bins for the data were determined based on the distribution shown in Figure 10. The num-

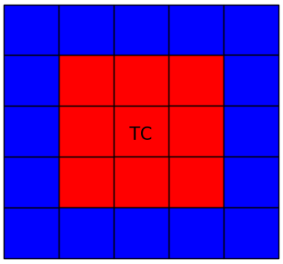

Figure 9. The two regions investigated around the TC: (1) the center of the TC and the closest eight 1° by 1° boxes surround the eye of the TC (shown in red) and (2) the 16 boxes 2° out from the TC center (shown in blue).

ber of points beyond ten lightning flashes decreases significantly in comparison to the data for zero through nine lightning flashes. Table 2 shows the number of occurrences on 10 October for each bin of lightning flashes from zero through nine and greater than nine. The middle column contains the number of flashes that occurred in the 1° by 1° boxes surrounding the TC center, marked in red in the upcoming analysis plots. The right column contains the data points for the occurrences in the boxes 2° out from the TC center, marked in blue in the upcoming plots.

For the precipitation data using the rainfall rate, two different binning intervals were compared. Figure 11 represents the data for all rainfall rate data points in comparison to the absolute value of the change in TEC. Based on the results in Figure 11, the bin sizes of the precipitation data were determined. The first calculation bins the data into 13 categories from zero increasing every 500 millimeters per hour (mm/hr), with the final category containing greater than or equal to 6,000 mm/hr. The second calculation bins the data from zero, increasing every 250 mm/hr into 21 categories, with the final category containing rainfall rates greater than or equal to 5,000 mm/hr. A variety of binning distributions were explored; however, the 500 mm/hr and 250 mm/hr intervals focus on where a majority of the data points are concentrated.

Table 3 shows the number of data points for each bin every 500 mm/hr. In the

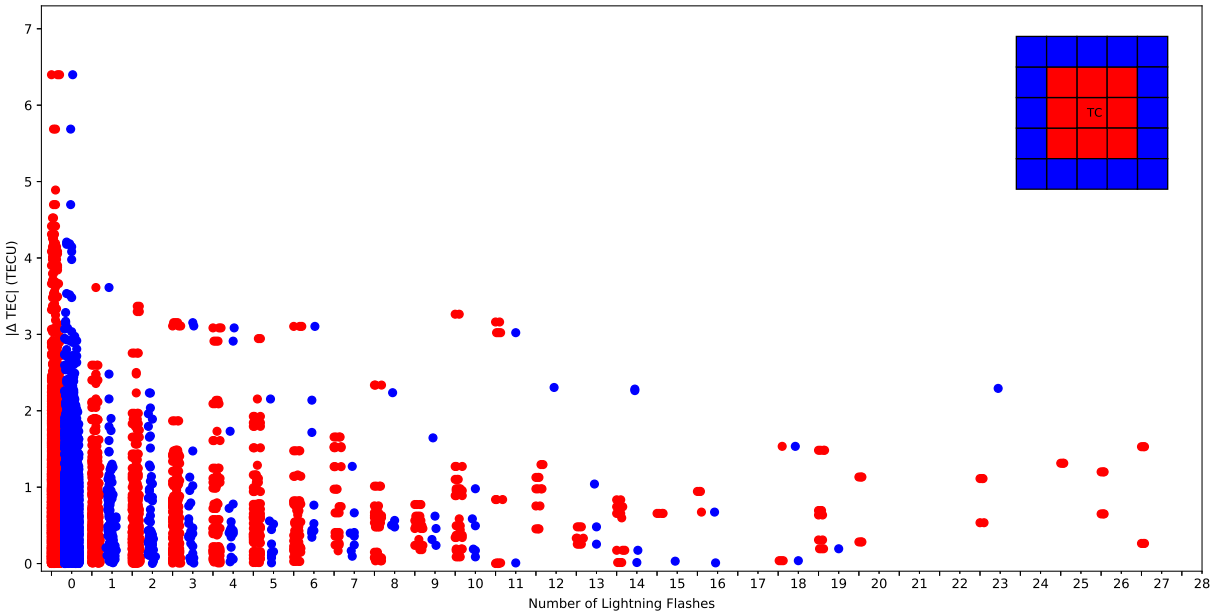

Figure 10. The lightning data used in this study for the corresponding number of lightning flashes based on the location of within 1° or 2° of the TC center to the absolute value of the change in TEC.

light rainfall rates, 0-1,500 mm/hr, there were more occurrences in the right column representing 2° out from the TC center. Beyond 1,500 mm/hr there were consistently more data points per category in the middle column representing the TC center and 1° out and including the TC center, with the exception of the 4,000-4,4999 mm/hr bin.

As with the previous table, Table 4 shows a distribution for the number of points used in the second calculations with rainfall rate bins of 250 mm/hr. From 1,250 mm/hr through 3,250 mm/hr there were consistently more data points per category in the middle column representing the TC center and 1° out from the TC center. Additionally, once the rainfall rate was above 3,000 mm/hr, the number of data points per bin decreased significantly.

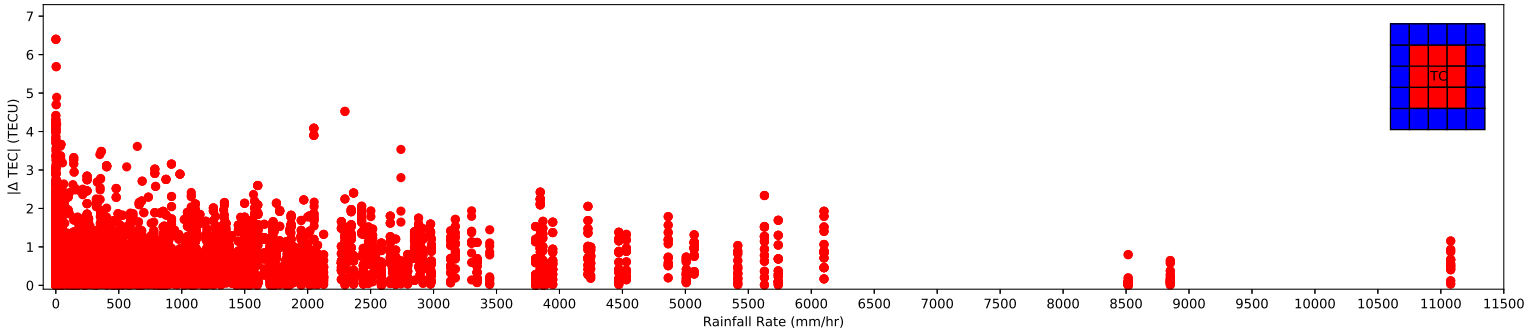

(a) Rainfall rate distribution for TC center and 1° out.

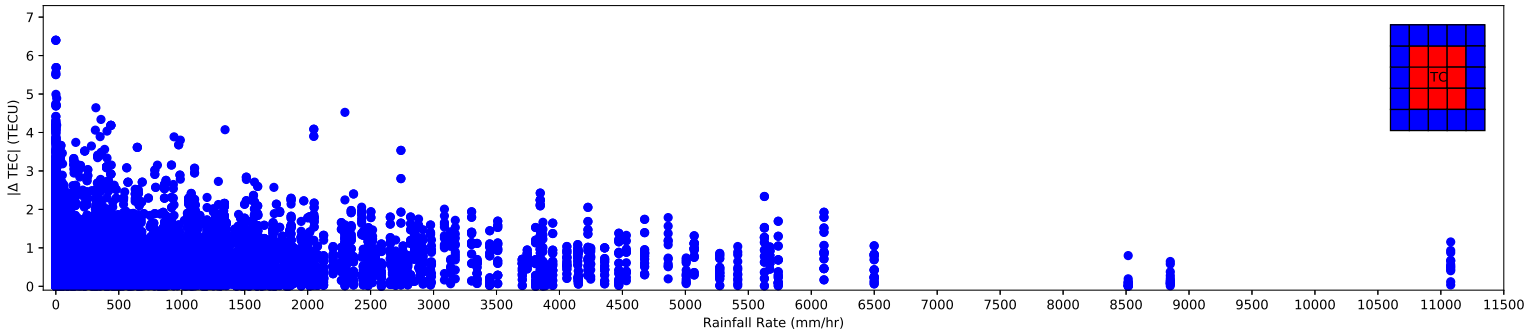

(b) Rainfall rate distribution for 2° out.

Figure 11. The precipitation data used in this study based on the location of within 1° or 2° of the TC center to the absolute value of the change in TEC.

Table 2. Number of lightning flashes used for the calculations to determine a relationship between lightning and the change in TEC. The left column contains the bins used, the middle column references the red points, and the right column references the blue points in Figure 9.

Number of Lightning Flashes	Red (1 deg box)	Blue (2 deg box)
0	10,409	19,622
1	592	739
2	303	329
3	213	202
4	119	123
5	127	94
6	77	69
7	33	33
8	41	24
9	23	19
> 9	141	110
Total	**12,078**	**21,364**

3.5 Boot Strapping Method

The bootstrap method is a statistical method that resamples data with replacement in order to estimate the variation of statistics being computed with the same data. To resample the data with replacement means that once a value is selected from a data set, it is placed back into the set, and the same value or point can appear multiple times within a resample. Moreover, the resample data set can be any size and can be resampled as many times as one desires or needs. This method is built on the law of large numbers; therefore, when a data set is resampled enough times, or has a large enough number of points, the empirical distribution of the data should be a good approximation for the true distribution (Efron and Tibshirani, 1986).

This method can be used for a variety of statistics even though it is commonly discussed in terms of the mean and variance. The resample of the data needs to be the same size as the original sample to be able to compute and compare the new, or empirical, distribution of the original sample to the bootstrap resamples. If the two samples are not the same size, then the empirical distribution value will not converge

Table 3. Number of data points for every 500 mm/hr rainfall rate range used for the calculations to determine a relationship between precipitation and the change in TEC. The left column contains the bins used, the middle column references the red points and the right column references the blue points in Figure 9.

Rainfall Rate Range	Red (1 deg box)	Blue (2 deg box)
0-499	6,655	15,279
500-999	1,615	2,408
1,000-1,499	1,252	1,665
1,500-1,999	972	768
2,000-2,499	447	357
2,500-2,999	429	287
3,000-3,499	108	96
3,500-3,999	192	144
4,000-4,499	96	132
4,500-4,999	48	48
5,000-5,499	84	60
5,500-5,999	72	48
$\geq$ 6,000	108	72
Total	**12,078**	**21,364**

with the original distribution, and it cannot be stated that the resample is a good approximation of the original (Efron and Tibshirani, 1986).

In this study, the bootstrap method was used to compute the error bars, or range of values for the TEC variability. For this method, the original data was resampled with replacement, creating an array of the same size as the original data, and repeating the resampling through 2,000 iterations. A median value was found for each of the 2,000 resamplings and subtracted from the median value of the original data. This new data of 2,000 points was used in the computation for a 90 percent confidence interval, plotted as the error bars. According to DiCiccio and Efron (1996),"two thousand bootstrap replications is 10 times too many for estimating a standard error, but not too many for the delicate tasks of setting confidence intervals."

Table 4. Number of data points for every 250 mm/hr rainfall rate range used for the calculations to determine a relationship between precipitation and the change in TEC. The left column contains the bins used, the middle column references the red points and the right column references the blue points in Figure 9.

Rainfall Rate Range	Red (1 deg box)	Blue (2 deg box)
0-249	5,676	13,555
250-499	979	1,724
500-749	829	1,385
750-999	786	1,023
1,000-1,249	662	902
1,250-1,499	590	763
1,500-1,749	540	516
1,750-1,999	432	252
2,000-2,249	197	154
2,250-2,499	250	203
2,500-2,749	201	131
2,750-2,999	228	156
3,000-3,249	48	36
3,250-3,499	60	60
3,500-3,749	0	72
3,750-3,999	192	72
4,000-4,249	60	96
4,250-4,499	36	36
4,500-4,749	24	36
4,750-4,999	24	12
$\geq$ 5,000	264	180
Total	**12,078**	**21,364**

IV. Analysis of Results

4.1 Overview

Analyses of the initial Total Electron Content (TEC) data are presented and then compared to two parameters, lightning and precipitation. First, the analysis of TEC for the region of the Gulf of Mexico and Southeastern US is presented as the raw data, then with a preliminary statistical analysis, followed by the Savitzky-Golay filter applied to remove the diurnal cycle from the data. Secondly, the lightning data is binned into 11 categories comparing the number of lightning flashes to the effects on the absolute value of the change in TEC ($|\Delta TEC|$). Finally, the precipitation data, through the rainfall rate, is compared with two analyses for bins of every 500 mm/hr and 250 mm/hr, to determine what groupings of rainfall rates have the greatest impact on the absolute value of the change in TEC.

There is no significant solar activity or solar flares to report during the time frame of Hurricane Michael, which could have contributed to influencing the TEC. Figure 12 shows the GOES X-Ray Flux product from NOAA/Space Weather Prediction Center (SWPC), which is used to track solar activity and solar flares. The red and yellow lines represent long passbands from the GOES–15 and –14 satellites, respectively, for 1.0-8.0 Angstroms. The blue and purples lines represent short passbands for the same satellites, respectively, for 0.5-4.0 Angstroms. Typically, SWPC does not send out space weather alerts unless the flare is within the M class band (Space Weather Prediction Center, 2018).

4.2 Total Electron Content Results

The TEC values over the five locations of Hurricane Michael on 10 October 2018 are compared for the 25 days leading up to the TC, through the lifespan of

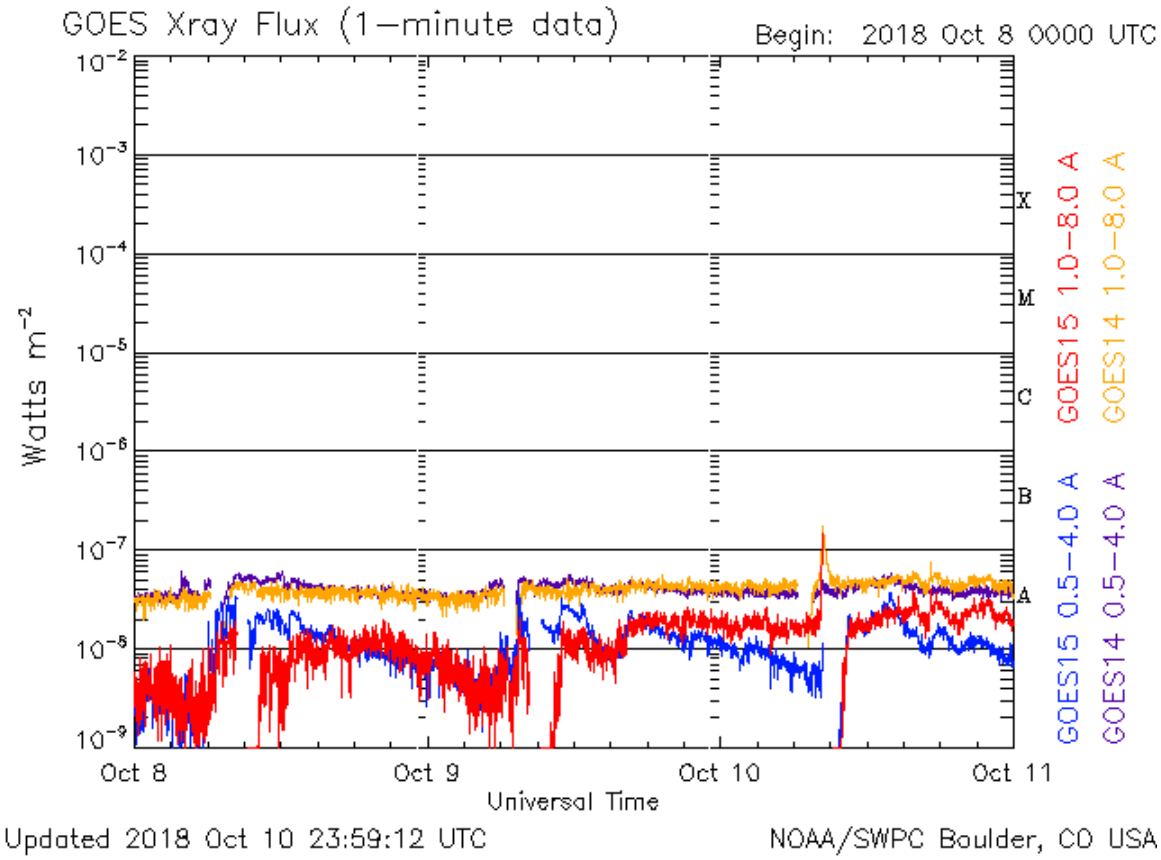

Figure 12. Representation of the X-Ray Flux tracking solar activity and solar flares for 8 to 11 October 2018. The red and yellow lines represent long passbands from the GOES–15 and –14 satellites, respectively, for 1.0-8.0 Angstroms. The blue and purples lines represent short passbands for the same satellites, respectively, for 0.5-4.0 Angstroms. Courtesy of NOAA/SWPC (Space Weather Prediction Center, 2018).

Hurricane Michael, and 6 days following the TC. This analysis provides an overview of the daily diurnal cycle and relatively "normal" conditions for how TEC fluctuates naturally on a daily basis for these locations, how those values change during a TC, and how they behave following the event. Figure 13 displays this analysis with the five points being shown in five colors, with the vertical black lines designating the time frame of Hurricane Michael, and the yellow highlighted area putting emphasis on 10 October, the main focus for this study.

During the 25 days leading up to Hurricane Michael, there are sporadic peaks in TEC values; however, the maximum values in general remain between 10.0-12.5 TEC

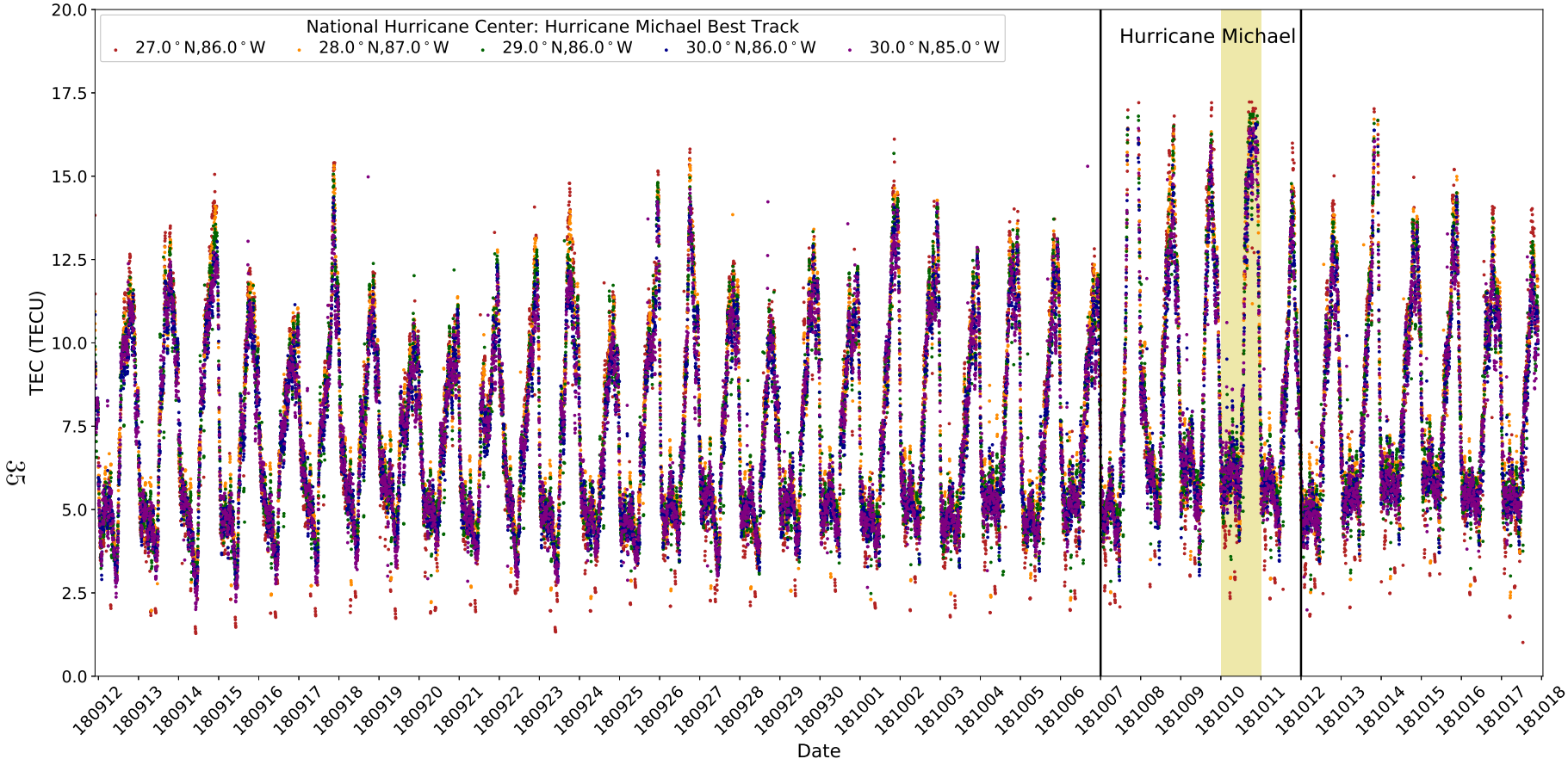

Figure 13. TEC data for the five points (five colors), from 10 October 2018 (yellow highlighted area), along Hurricane Michael's track for the 25 days leading up to the TC, 5 days during (designated by the black vertical lines), and 6 days following. There are sporadic higher peaks in TEC values during the 25 days leading up to Hurricane Michael; however, during the time Hurricane Michael is occurring, there is a maintained increase in the maximum TEC values each day, as well as higher minimums. Furthermore, overall the range of values decreases once again back to pre-TC levels in the 6 days following Hurricane Michael. These results are one indication of Hurricane Michael having an influence on the ionosphere and TEC values.

Units (TECU). In comparison, during Hurricane Michael, the peak values increased to approximately 17.0 TECU and remain sustained for the days of the TC (7-11 October), with the greatest concentration of TEC points and highest values occurring on 10 October, when the TC rapidly intensified and reached its peak intensity. Following Hurricane Michael, the values return back to relatively "normal" values with maximums near 12.5 TECU. These results are one indication that Hurricane Michael had an influence on the ionosphere and TEC values.

In order to confirm these results further—that Hurricane Michael is indicative of being a cause for fluctuations in TEC—data from a relatively calm, high pressure weather day, with no significant solar or geomagnetic activity to report (19 September 2018) is compared to Hurricane Michael's peak intensity on 10 October 2018. The GOES X-Ray Flux for 19 September in Figure 23 and the surface weather maps for both days are found in Figure 24 in Appendix A.

Figure 14 compares one standard deviation for both days and Figure 15 compares the median TEC values. The standard deviation and median values are computed for each 1° by 1° box for each day (288 time steps per day). Both Figures 14 and 15 are plan views of the Gulf of Mexico and the Southeastern US. For these figures, the area is expanded beyond that seen for the majority of the study, as outlined by the green box in Figure 8, because on 10 October, there was a cold front with embedded thunderstorms moving through eastern Texas into Louisiana (shown in the surface weather map in Figure 24b in Appendix A). Based on the previous research studies discussed in Chapter II, expanding the map view allows for the evaluation for similarities or differences in the TEC results due to the TC and the cold front.

In Figure 14, the relatively larger values are seen in the southern half of the Gulf of Mexico into the Caribbean Sea for both days. This is likely due to missing data, as these areas are further away from the CORS receivers (ref. Chapter III).

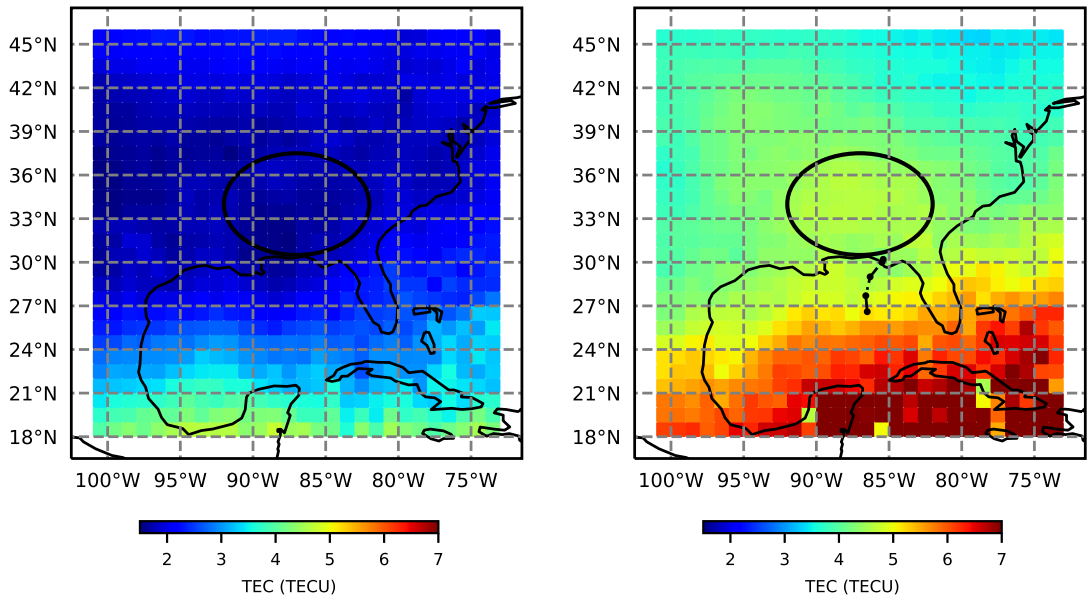

(a) 19 September 2018 **(b) 10 October 2018**

Figure 14. Plan view of one standard deviation for the area of interest for (a) 19 September 2018 and (b) 10 October 2018. Hurricane Michael's path on 10 October is indicated by the black dots and dotted lines in the northern Gulf of Mexico. The color bar on the bottom indicates the TEC value for each box of 1° latitude by 1° longitude. The circled area over the Southeastern US highlights an area of increased standard deviation values in October versus September, consistent with Hurricane Michael playing a role in higher TEC.

Additionally, these regions are closer to the equator, therefore, higher values within those regions are to be expected. Looking more closely at 25°N and north, in the circled areas, the standard deviation values on 19 September are approximately 2.0 TECU, while on 10 October the values are approximately 5.0 TECU. As the scale is the same for both figures, the southern nine degrees of latitude are not skewing the colors shown in this Figure, and the circled area is mainly to the north and over the area of Hurricane Michael. This comparison is also completed for other days leading up to Hurricane Michael with similar results, found in Appendix A.

Figure 15 shows the results for the median TEC value for both days. These results are more consistent between the two days, compared to Figure 14, with median values of 4.0-5.5 TECU spanning a large portion of the Southeastern US and the

southern Gulf of Mexico into the Caribbean Sea. The portion in eastern Texas and the western Gulf of Mexico are consistently approximately 6.5-7.0 TECU regardless of the day. Figures displaying the results for additional days leading up to Hurricane Michael are found in Appendix A.

The areas circled in Figure 15 show the sharp comparison from values of 5.5-6.0 TECU on 19 September and 7.0-7.5 on 10 October. These areas are consistent with rainbands extending out in a spiralling manner from the center of Hurricane Michael on 10 October, as seen in the satellite image of the storm (Figure 7).

4.1.1 Savitzky-Golay Filter Applied

Next, to remove the diurnal cycle shown in the TEC data in Figure 13, the Savitzky-Golay filter is applied. This allows the deviations to be centered around zero. As mentioned in Chapter III, for this study, a six-hour window and 3rd order polynomial are used in the Savitzky-Golay filter.

Following the Savitzky-Golay filter application, this 36-day window is evaluated using one standard deviation for each five-day segment of days, and the last segment with 6 days following Hurricane Michel. These seven segments for each point are shown as horizontal lines in Figure 16, with the five colors representing the five points from 10 October 2018 (yellow highlighted area), with the time frame of Hurricane Michael being designated by the black vertical lines. The dots show the change in TEC (ΔTEC) values after the filter is applied, with the change in TEC now on the vertical axis. For all five best track points, the standard deviation values increased during the time frame of Hurricane Michael, and decreased even more after the TC than values prior to the TC, again indicative of Hurricane Michael having an influence on TEC.

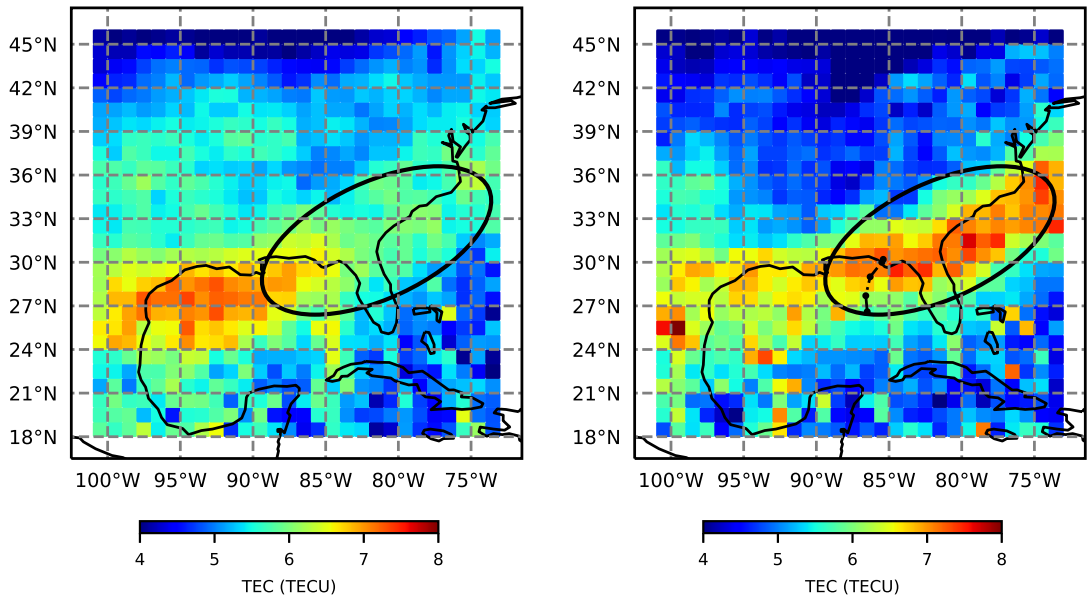

(a) 19 September 2018 **(b) 10 October 2018**

Figure 15. Plan view of the median TEC values for the area of interest for (a) 19 September 2018 and (b) 10 October 2018. Hurricane Michael's path on 10 October is indicated by the black dots and dotted lines in the northern Gulf of Mexico. The color bar on the bottom indicates the TEC value for each box of 1° latitude by 1° longitude. The circled area highlights an area of increased median TEC values in October versus September.

4.2 Lightning Results

The first parameter investigated to explore the influence of Hurricane Michael on TEC is lightning. Lightning is an electric component of a TC and is more common in the rainbands of a TC, in comparison to the eye wall of the storm (ref. Chapter II). Figure 17 shows a compilation of all the lightning flashes within the Gulf of Mexico and Southeastern US on 10 October 2018. There is a concentration of flashes along Hurricane Michael's path, marked and labeled in black. As these are lightning flashes from the entire day, it is not conclusive from this figure to argue that the flashes occurred directly around the eye of the storm. Rather, these lightning flashes are likely caused from the storm moving throughout the day. Furthermore, lightning from the rainbands can be identified stretching out from the center of the storm along

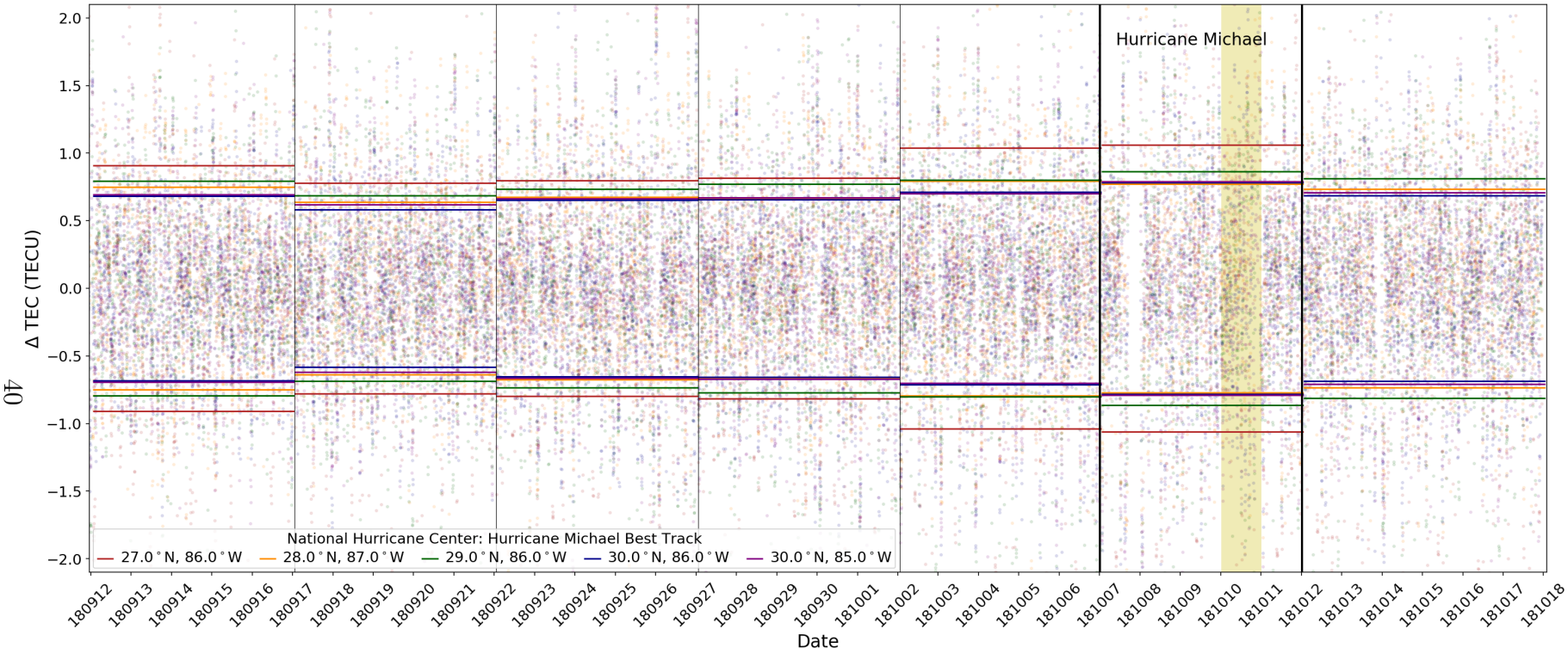

Figure 16. TEC data for the five points (five colors) from 10 October 2018 (yellow highlighted area), along Hurricane Michael's track for the 25 days leading up to the hurricane, 5 days during (designated by the black vertical lines), and 6 days following. The standard deviation is taken for every five-day segment through the 36 days, with the last segment containing the six days following Hurricane Michael.

Hurricane Michael's path.

Next, the lightning flashes that are concentrated along Hurricane Michael's path stretching east-northeast across Florida and northeast towards South Carolina match up well with the outlined area in Figure 15b, which shows a concentrated increase in TEC on 10 October. With this relationship identified, a correlation is investigated relating the number of lightning flashes to the absolute value of the change in TEC. This allows the vertical axis of the results to be all positive values, rather than the results being centered about zero (ref. Figure 16). These results are built off the distribution of the data in Figure 10, which shows significantly less occurrences when there are more than 10 lightning flashes.

The distribution of values in Figure 10 and Table 2 are used to calculated the median values and in the bootstrap resampling for the results in Figure 18. For example, the calculations for the black dot on the red line at zero lightning flashes is the median value from 10,409 data points, and the error bars for that point are computed through the bootstrap method with 2,000 resamples for a 90 percent confidence interval. The black dots and stars are the median values for each of the bins of data, with the stars indicating median values larger than that at zero lightning flashes for the designated color. The median values at zero lighting flashes are shown with the horizontal red and blue lines, respectively, and at nearly the same value for this plot, at approximately 0.52 TECU. These horizontal lines are a reference for where the black stars are derived from. As mentioned in the example, the error bars on this plot are calculated through the bootstrap method with 2,000 resamples for a 90 percent confidence interval.

In Figure 18, the median values are fluctuating with the variation in the number of lightning flashes, but do not show a consistent trend. Likewise, the bounds of the error bars are not conclusive in showing that increasing the number of lightning flashes

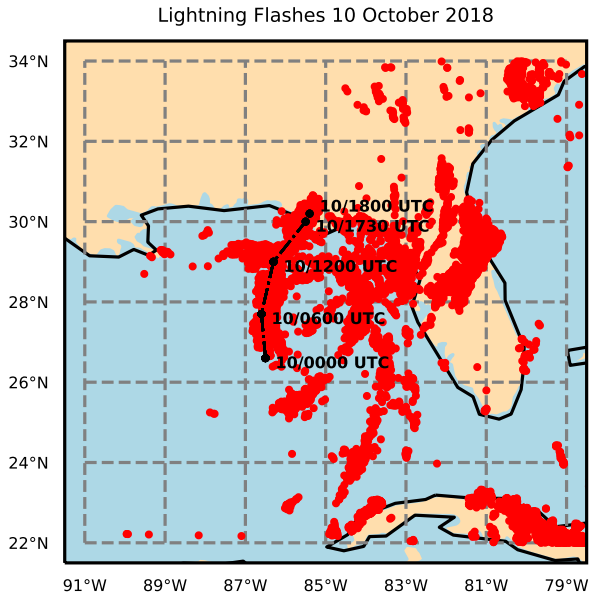

Figure 17. A plan view of the Gulf of Mexico with Hurricane Michael's path on 10 October 2018 shown in black and all the lightning flashes from that day shown in red.

results in an increase in the absolute value of the change in TEC. In regards to the red error bars associated with seven lightning flashes, even though there are 33 data points incorporated into the bootstrap resampling, the range of initial values is 0.167 to 1.656, with 13 of the values being greater than 1.2 TECU. These results suggest that seven lightning flashes may be a number where the TEC value is likely to be higher; however, this is not likely for these results considering how much lower the surrounding median values are, as well as the ranges of the other values. It is not clear why this particular result is in favor of such high TEC fluctuations. In comparison, for eight lightning flashes (at 1°out and the eye) there are 41 data points, with seven greater than 1.0 TECU and three greater than 2.0 TECU, and for greater than nine lightning flashes there are 141 data points with 31 occurrences greater than 1.0 TECU, but less than 1.5 TECU, and seven points greater than 3.0 TECU, with these medians being less than the median at seven flashes.

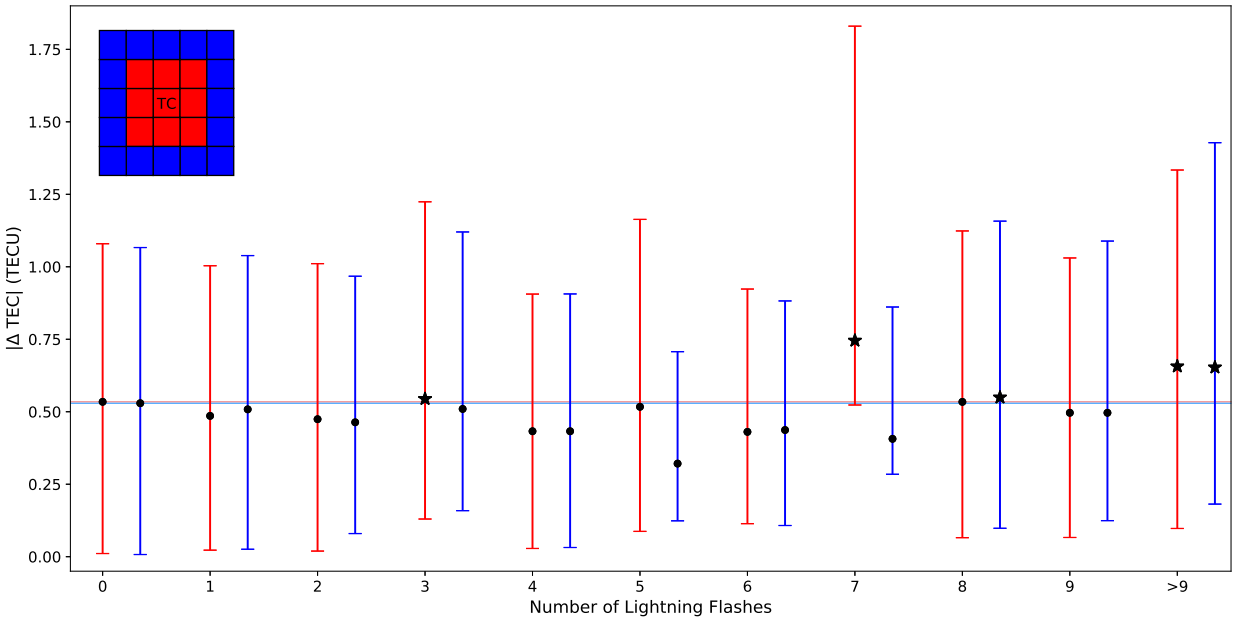

Figure 18. The results of the number of lightning flashes in comparison to the absolute value of the change in TEC. The black dots and stars are the median values for each of the bins of data (i.e. number of lightning flashes), with the stars indicating median values larger than that at zero lightning flashes for the designated color. The median values at zero lighting flashes are shown with the horizontal red and blue lines, respectively, and at nearly the same value for this plot, at approximately 0.52 TECU. The error bars on this plot are calculated through the bootstrap method with 2,000 resamples for a 90 percent confidence interval. Overall, the median values are fluctuating with the variation in the number of lightning flashes, but do not show a consistent trend and the bounds of the error bars are not conclusive in showing that increasing the number of lightning flashes results in an increase in the absolute value of the change in TEC.

4.3 Precipitation Results

The second parameter investigated is precipitation as rainfall rate. Precipitation is a dynamic component of a TC, and is used as a proxy for convective activity. In a TC heavier precipitation is expected in the eye wall and in the front or front-right quadrant of the storm, relative to the direction of travel. Figure 19 shows a plan view of the rainfall rate at 18:00 UTC on 10 October, just following Hurricane Michael making land fall with the concentration of heaviest precipitation being consistent

with where it is expected. Hurricane Michael's path for 10 October is shown with the black dots and dotted line, and regions that are dark red (the far right side of the color bar) are greater than or equal to 5,700 mm/hr. The two disconnected areas from the greatest rainfall rate, off the east coast of Florida and into South Carolina, as well as the area extending south along the west coast of Florida are representative of areas of precipitation due to the spiraling rainbands.

The values from Table 3 are used to calculated the median values and error bars through the bootstrap method for the first analysis of the precipitation data, with intervals every 500 mm/hr. Figure 20 is structured the same way as Figure 18 with regards to the representation of the colors, black dots, and error bars. For

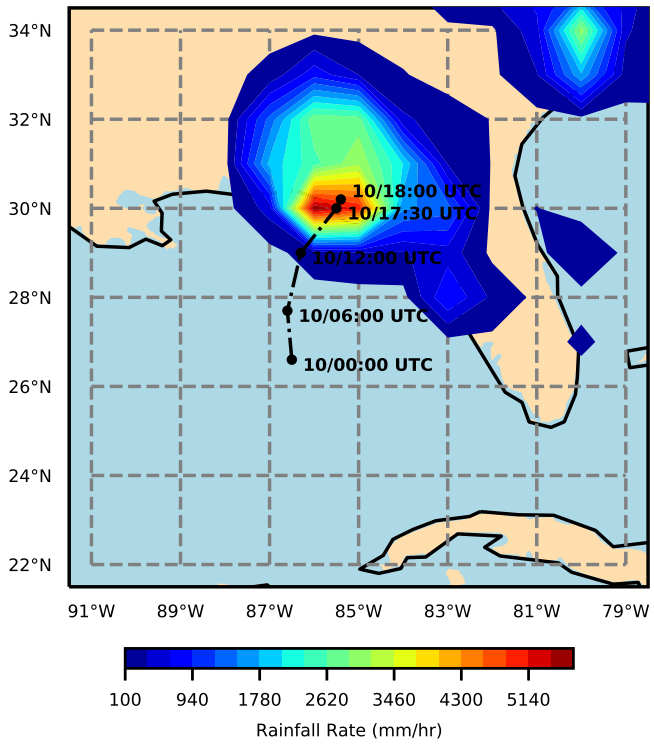

Figure 19. A plan view of the Gulf of Mexico and Southeastern US with Hurricane Michael's path on 10 October shown in black and the rainfall rate at 18:00 UTC, with regions in the dark red (the far right side of the color bar) being greater than or equal to 5,700 mm/hr. The heaviest precipitation is found over the TC center location as well as extending into the front and front-right quadrant, as expected.

the rainfall rate, the black stars are the median values larger than that for the 0-499 mm/hr rainfall rate bin for the designated color. The median values for this lowest bin are shown with the horizontal red and blue lines.

Figure 20 shows an increase in the median values for both 1° and 2° out from the TC center for light to moderate rainfall rates. For the purposes of this study, light rainfall rates are defined as 2,000 mm/hr or less, moderate as 2,000-5,000 mm/hr, and heavy rainfall rates as greater than 5,000 mm/hr. The greatest increase for both the median values and the range of values represented by the error bars, is highlighted by the gray arrow from 1,500 to 3,000 mm/hr. There is a continuation of the increase

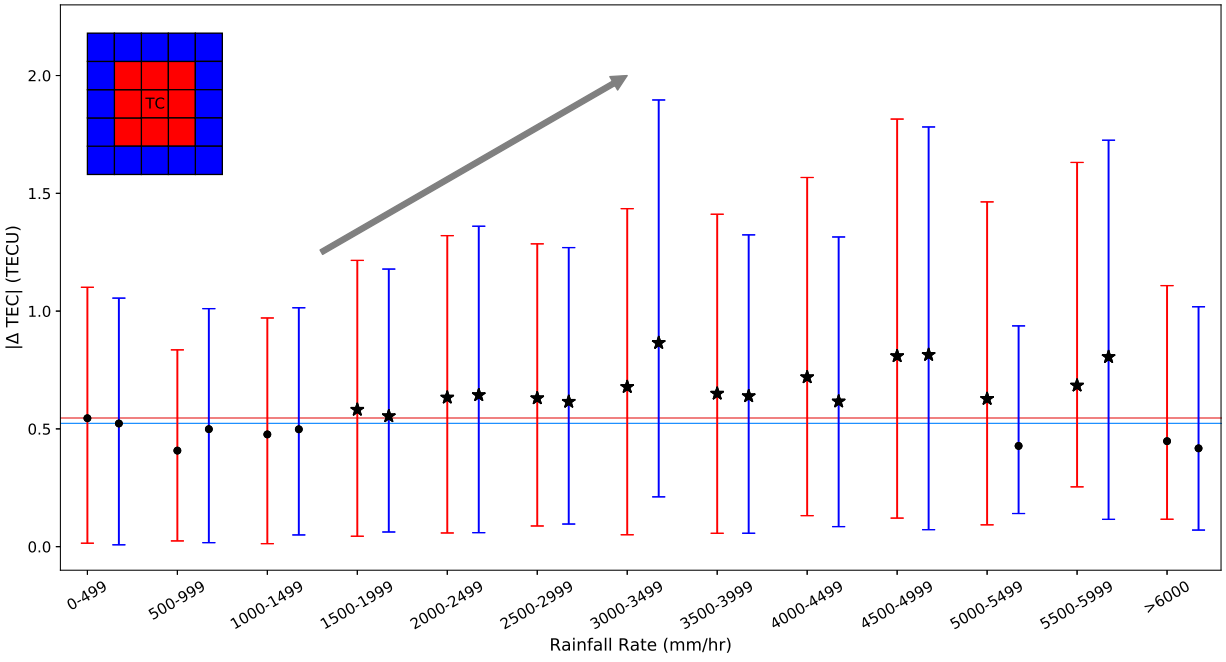

Figure 20. The results of varying rainfall rate bins for every 500 mm/hr in comparison to the absolute value of the change in TEC. The descriptions for the box in the top left, black dots, colors, and error bars can all be referenced in the caption for Figure 18. The black stars are median values larger than that for the 0-499 mm/hr rainfall rate bin for the designated color. The median values for this lowest bin are shown with the horizontal red and blue lines, with the values at approximately 0.55 and 0.52 TECU, respectively. In this figure, the median values, as well as the ranges for the error bars, are increasing with a light to moderate rainfall rate (i.e. 1,500-5,000 mm/hr). The greatest increase is highlighted by the gray arrow from 1,500-3,000 mm/hr.

for the red points, at the TC eye and 1° out, up through 5,000 mm/hr. The relatively abnormal high median and range of values for the 2° out blue points for the bin from 3,000-3,499 mm/hr is not clear for the reason behind these higher values. One potential contributing factor may be that there are 96 data points, which is less points relatively to those surrounding that bin, even though this should not influence the results as a potential error when using the bootstrap method to resample the data.

The second analysis for the precipitation data consists of bins every 250 mm/hr, with the data distribution from Table 4 used for the median and bootstrap calculations. Figure 21 shows this analysis taking a closer look at the bins that are in the range of increasing values for the first precipitation analysis (ref. Figure 20).

In comparison to Figure 20, Figure 21 shows the same increasing trend for light to moderate rainfall rate from 1,500 to 3,000 mm/hr; however, with these smaller bin sizes, there is not as clear of a continuous increase in the red values beyond 3,000 mm/hr. There is a drop in the median TEC values from 3,500 to 4,500 mm/hr, yet the median TEC values are still greater than that for the 0-499 mm/hr bin, and the magnitude of the ranges of values for the error bars are also less. The range for the error bars increase in three out of the four last bins—4,250-4,999 mm/hr—for all three red lines, and two of the blues lines. For these calculations, there are 36 points or less for each of the groupings, potentially adding to the uncertainty of how these rainfall rates contribute to the change in TEC. The last bin for greater than or equal to 5,000 mm/hr contains median TEC values less than those in the 0-499 mm/hr bin indicative of a potential threshold where heavy rainfall rates do not equate to an additional increase in the change in TEC.

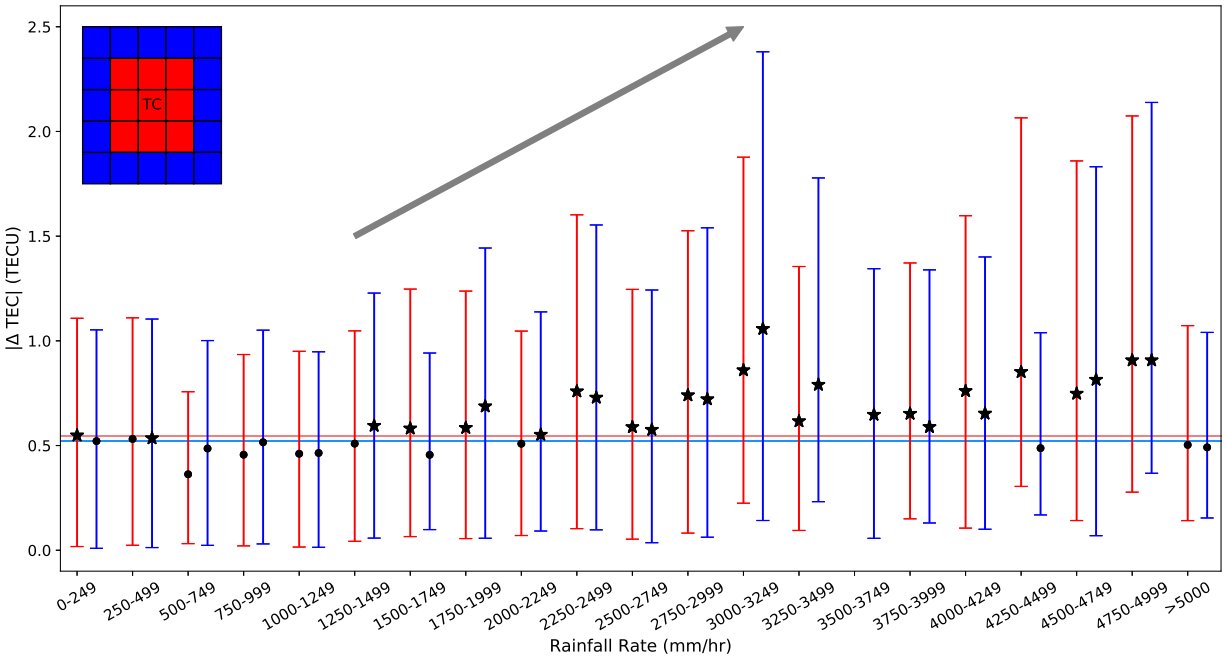

Figure 21. The results of varying the rainfall rate bins by 250 mm/hr in comparison to the absolute value of the change in TEC. The descriptions for the box in the top left, black dots, colors, and error bars can all be referenced in the caption for Figure 18 and the black stars from Figure 20. Overall, the median values and the range for the error bars are increasing with a light to moderate rainfall rate (i.e. 1,500-5,000 mm/hr). The bins of 250 mm/hr, in comparison to every 500 mm/hr, allows for a closer look to where the light to moderate rainfall rate is no longer contributing to an increasing TEC value trend. In these results, as compared to Figure 20, there is a drop in the values from having a consistent increase from 3,250 to 4,500 mm/hr, though the median values are still greater than that for the 0-499 mm/hr bin, the ranges of values for the error bars are less.

V. Discussion and Conclusions

5.1 Discussion

There are multiple indications of Total Electron Content (TEC) being impacted by Hurricane Michael, especially with no significant solar activity to report during the storm's time frame. First, the results in Figure 13 are an indication of Hurricane Michael causing a disturbance in the ionosphere and fluctuations in TEC with the increase in TEC observed during the time frame of Hurricane Michael and the decrease in the values following the storm. There are sporadic peaks with higher TEC during the 25 days leading up to Hurricane Michael; however, the persistence and maximum values during the storm time frame are significant indicators of the impact the storm caused. These results are consistent with the results from the study by Polyakova and Perevalova (2013)—the greatest TEC variations were observed when the TCs were most intense. The reason for the sporadic peaks before Hurricane Michael is not clear because there was no significant solar activity or significant weather. It is possible that larger convective systems, such as a low pressure systems or cold front passing through the Gulf of Mexico, are the cause behind these sporadic increases; however, an in-depth assessment of these peaks is not conducted as part of this study.

Second, in comparing the plan views of 19 September—a calm day prior to Hurricane Michael—and 10 October—when the TC was most intense—(Figures 14 and 15), the vast difference in the state of the ionosphere is shown. On 10 October, the ionosphere is already modified by the influences of Hurricane Michael from the three days prior as the TC developed and intensified. These results are consistent with the study by Polyakova and Perevalova (2011), where the longer the period of variation observed, the greater the TEC variation amplitude. Looking at the days surrounds Hurricane Michael, allows the observation of TEC fluctuations that do

not appear immediately. This is a reason why the standard deviation of TEC on 19 September is approximately 2.0-3.0 TECU for majority of the plan view area and why on 10 October it is approximately 4.0-5.0 TECU. This is consistent with the median TEC increasing by approximately 1.0-1.5 TECU on 10 October.

Finally, in Figure 16, the Savitzky-Golay filter removes the diurnal trend from the TEC, and one standard deviation is calculated for the sections of dates (before, during, and after Hurricane Michael) indicating the same results of higher values during the TC. There is an increase in standard deviation from each five-day segment leading up to Hurricane Michael compared to during the TC. It is not clear from this study what may be the cause of the relatively higher TC standard deviation the last five-day segment prior to the storm forming; however, these results are an additional confirmation to explore the TC parameters that may be the reasons behind the fluctuations in TEC.

Lightning is the first parameter explored without conclusive results. The median TEC values and error bar ranges for each set of data do fluctuate; however, with no clear trend identified for some or more lightning being consistent with an increase in TEC. From Figure 10, it is clear to see that the greatest changes in TEC are with no lightning occurrence at all, but there are still a moderate amount of changes in TEC for one through six lightning flashes with the TEC reaching approximately 2.0-3.0 TECU for more than just a few outlier results, such as in ten or eleven lightning flashes. With the indication that some lightning (i.e. one to six lightning flashes) does show a greater increase in the change in TEC, some correlation or connection may be found between this TC parameter and the TEC variations, with further investigation.

Since there are typically more lightning flashes in the outer rainbands of a TC, the expectation is to see more flashes, and thus a greater influence to TEC in the blue lines, for 2° out from the TC center, for greater than zero lightning flashes in

Figures 10 and 18. This expectation is not met, as the results in Figure 18 show the median values and error bar ranges decreasing through seven lightning flashes for 2° out. Furthermore, the results are not compelling based on the spread of values for the bins, such as for the red line at seven lightning flashes (ref. Chapter IV). From the calculations completed and the results in this study, varying the number of lightning flashes still leaves uncertainty and is inconclusive for this parameter being the cause of TEC variations.

The second parameter investigated is precipitation through rainfall rates as a proxy for convection. The heaviest precipitation, or greatest rainfall rate, is frequently in the eye wall of a TC and in the front or front-right quadrant of the storm, relative to the direction it is traveling, consistent with the results in Figure 19. The distribution of rainfall rate to the absolute value of the change in TEC (Figure 11) shows a large concentration of data points in the light (0-1,500 mm/hr) to moderate (1,500-3,000 mm/hr) rainfall rates. In general, the expectation for the distribution of rainfall rates for a TC is to see a greater concentration of data points in the higher values of rainfall rate for the red data points, for the TC eye and boxes 1° out. In Figure 11, however, the distribution for rainfall rates appears as fairly balanced and consistent from Figure 11a for 1° out and Figure 11b for 2° out.

Next, in Figure 20, a more consolidated view of the rainfall rate results for data binned every 500 mm/hr, shows an identifiable trend in the data with the median TEC values and the ranges of values for the error bars consistently increasing from 1,500 mm/hr to 3,000 mm/hr for both the red and blue lines, with the red 1° out values continuing to increase through 5,000 mm/hr. From these results, the lighter rainfall rates (up to 1,500 mm/hr) show a decrease in TEC variation; however, for the moderate rainfall rates, a relationship between rainfall rate and TEC variations is established.

To further analyze the rainfall rate results, the data is divided up further into bins for every 250 mm/hr. Figure 21 shows a closer look at the threshold of rainfall rates where TEC variation is increasing. The range of increasing values is expanded from 1,250 mm/hr to 3,250 mm/hr for both the red and the blue lines with a drop in the trend following above 3,250 mm/hr. During this drop, the rainfall rates are still greater than those for the lowest bin, signifying that even if it is not the greatest TEC variation, the TEC is still affected by rainfall rates within the TC. As mentioned above, Tables 3 and 4 show that there are in fact more data points in the blue, boxes 2° out, section rather than closer to the core of the TC.

Even though the precipitation results show very high rainfall rates, which if sustained would result in tens of inches of rain, the rainfall rates are related to the intensity of precipitation in the TC. Figure 22 shows the total rainfall analysis for Hurricane Michael from the NHC Hurricane Michael storm analysis (Beven II et al., 2019). These results are consistent with those in Figure 19, with significant rainfall along the coast of Florida in the Gulf of Mexico, where Hurricane Michael made landfall. This comparison is important, highlighting that total precipitation tells the same story as the rainfall rate, which may be short-lived at times during the TC or persistent at other times.

5.2 Limitations

5.2.1 Methodology Limitations

The results from applying the Savitzky-Golay filter may be impacted where the data points are not uniformly spaced in time due to the nature of a moving window (Press and Teukolsky, 1990). In this case study, the data points in time that did not have a TEC value—not a number (NAN) in regards to programming—were removed prior to applying the Savitzky-Golay filter, removing the respective time intervals for

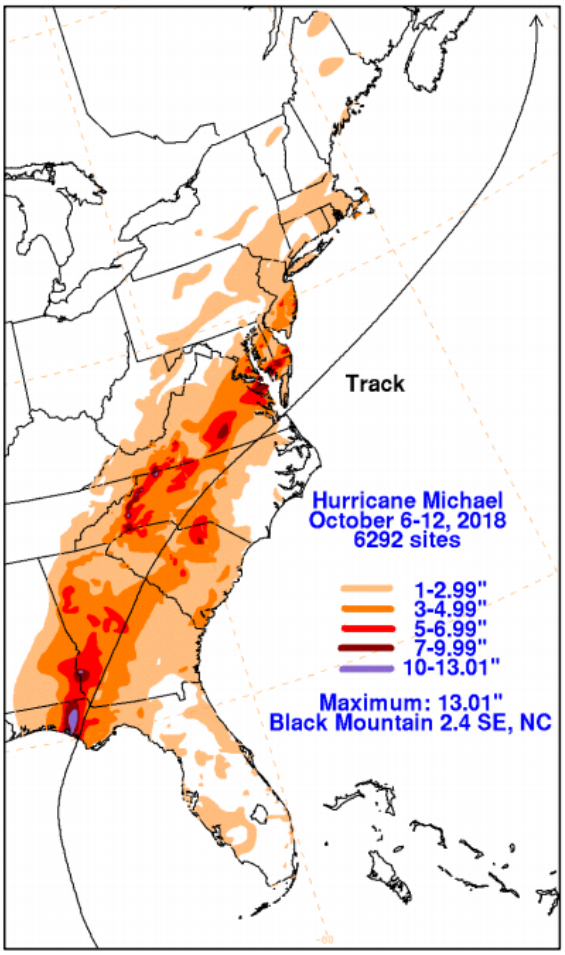

Figure 22. Analysis of storm total rainfall (inches) for Hurricane Michael. Courtesy of David Roth of the NOAA Weather Prediction Center (Beven II et al., 2019).

the window along the way. These calculations, with missing time steps, may have skewed the results, but when the NAN data points were not removed the filtered results did not match up with the data. These limitations are mainly due to missing data in the Gulf of Mexico further away from CORS receivers or due to interruptions in connectivity for data reporting between the satellite and receiver, likely caused by the changes in the ionosphere.

5.2.2 Data Limitations

For the TEC data, there are two main limitations. First, even though there are a vast amount of GPS receivers in the US along the coast of the Gulf of Mexico (ref. Figure 6), the further away the grid box is from the Continuously Operating Receiver Stations, the more holes there are in the data. Second, if signals get delayed or interrupted while transmitting between satellite and receiver due to the TC, or other factors contributing to TEC variations, this can cause missing data in regions where at most time steps there would be a TEC value. At this point, with this data set, it is not possible to interpolate or receive an accurate TEC value without guessing for these grid boxes or time steps, especially if the signal is interrupted.

Next, in regards to the lightning data, utilizing the data from the GLM may be a limitation due to the detection efficiency range, the newness of the data set, and the lightning location accuracy. First, the lightning flash detection efficiency is affected by day and night, with the GLM having a minimum detection efficiency of 70 percent, regardless of the time of day. The efficiency increases during the nighttime, when the sunlight is not creating a reflection as background noise for the GLM. This reflection of sunlight creates an increased uncertainty during the daytime; however, the GLM algorithm does utilize four filtering technique to attempt to minimize these effects. More details on the filtering techniques can be found in Goodman et al. (2012a). Second, GLM for the GOES–16 satellite began reporting in March 2017. This data has not been verified or utilized in as many studies as other lightning data sets due to the more recent launch of this instrument. Third, according to Goodman et al. (2012a), the lightning location accuracy is within 5 km. This does not impact this study quite as much since each 1° by 1° box is approximately 110 km by 90 km; however, the accuracy of the lightning flashes can play a role for where the TEC impacts are located.

Lastly, the precipitation data uses the rainfall rate as a proxy for convective activity. This convective activity is identifying regions with stronger updrafts leading to a stronger TC structure, rather than convective activity in the sense of embedded thunderstorms with lightning. Using this data set as a proxy is a limitation since it is not an accurate measure of the variable being explored. Additionally, since the rainfall rate is hourly, it is a limitation when comparing 12 TEC values in an hour per grid box to only one rainfall rate value.

5.3 Future Work

This is one case study exploring the relationship between two TC parameters and the change in TEC. One case study is not enough to describe the relationship between TCs and TEC variation with confidence; hence, more case studies need to be conducted. Furthermore, exploring additional TC parameters, TCs in other basins of the world, and working to find a method to utilize TEC changes to observe rapid intensification of a TC, are all items to be examined in the future to overcome some of the shortfalls of this study.

Also, the lightning data used in this study is only one of many. Using different lightning data in the future may allow for a comparison to confirm or counter the results that lightning, as an electrical component of a TC, is not the main cause of TEC variations. The precipitation data is used as a proxy for convective activity and stronger updrafts within a TC; therefore, investigating other variables for vertical motion and convective activity would be beneficial. To explore this, simulated model data may be a viable supplement to the observed data, especially since the observations themselves for TCs are limited due to the nature of the natural phenomenon. Furthermore, this study related rainfall rates to certain levels of TEC variation. Looking at other aspects of precipitation and tracking method for precipi-

tation are an additional avenues to explore.

After additional case studies and more conclusive results, TEC variations have the capacity to be utilized as a proxy for forecasting and monitoring TC generation and intensification. The GNSS data utilized in TEC calculations are readily available and can be used in a real time manner. With a gained understanding of what features can be identified in an intensifying or generating TC, such as spikes in TEC, these data can be an additional resource for forecasting these very disastrous phenomena, tropical cyclones. In addition, utilizing different data sources that characterize the state of the ionosphere will also provide another comparison, such as the MIT Haystack slant TEC.

5.4 Conclusions

The objective of this thesis is to determine if the various parameters of a TC can be identified as the causes for variation in TEC during Hurricane Michael (2018). Currently, there is an understanding on the impacts that TEC variations have on signals passing through the ionosphere and that tropospheric weather events do impact the state of the ionosphere and TEC.

While the results of this research are preliminary and require further validation through more case studies, they are indicative of Hurricane Michael, causing disturbances to the ionosphere. When comparing lightning to changes in TEC, the results are unconvincing of this parameter being the primary cause of TEC fluctuations during the time frame of Hurricane Michael. In contrast, the results for the rainfall rate as a proxy for convective active are more conclusive. There is a clearer trend in rainfall rates from 1,500 to 3,000 mm/hr showing an increase in the median TEC value and range of values for the error bars from the bootstrap resampling method. With further comparisons and calculations in the role of TC parameters in TEC fluc-

tuations, the techniques developed could be useful for forecasting TC development, identifying an occurrence of a large unplanned phenomenon (whether naturogenic or anthropogenic), and project impacts to communication systems during a TC.

Appendix A

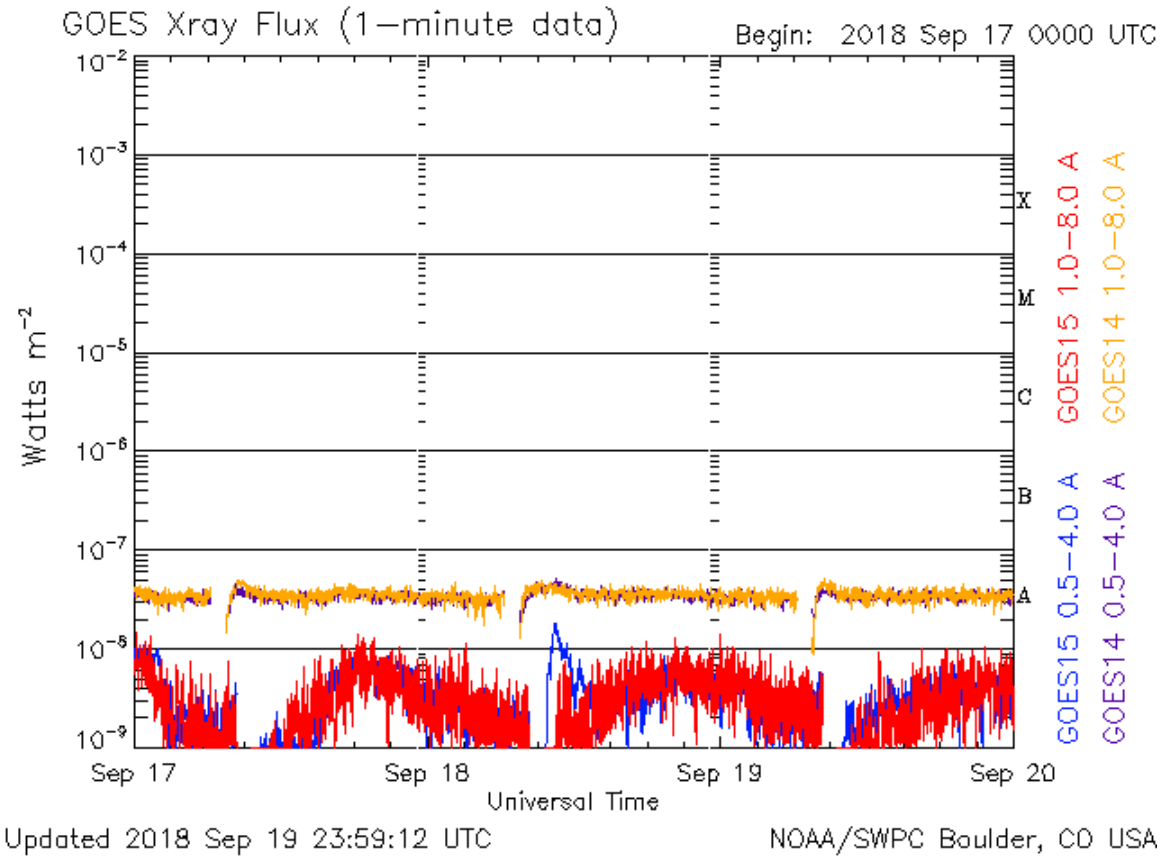

Figure 23. GOES X-Ray Flux for 19 September 2018, the day used for comparison to 10 October 2018 in Chapter IV. No significant space weather impacts to report. Courtesy of NOAA/SWPC (Space Weather Prediction Center, 2018).

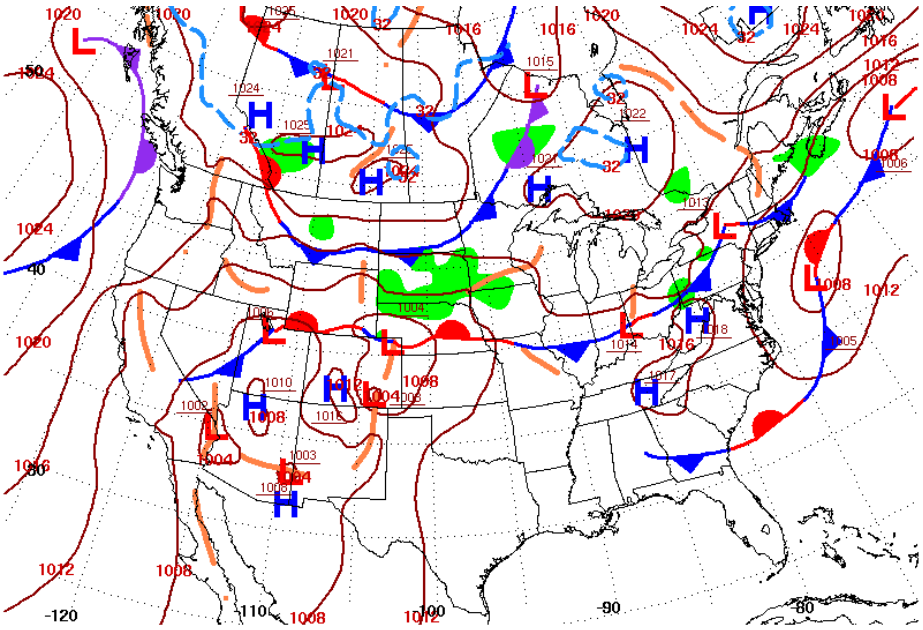

(a) Surface weather map analysis for 19 September 2018

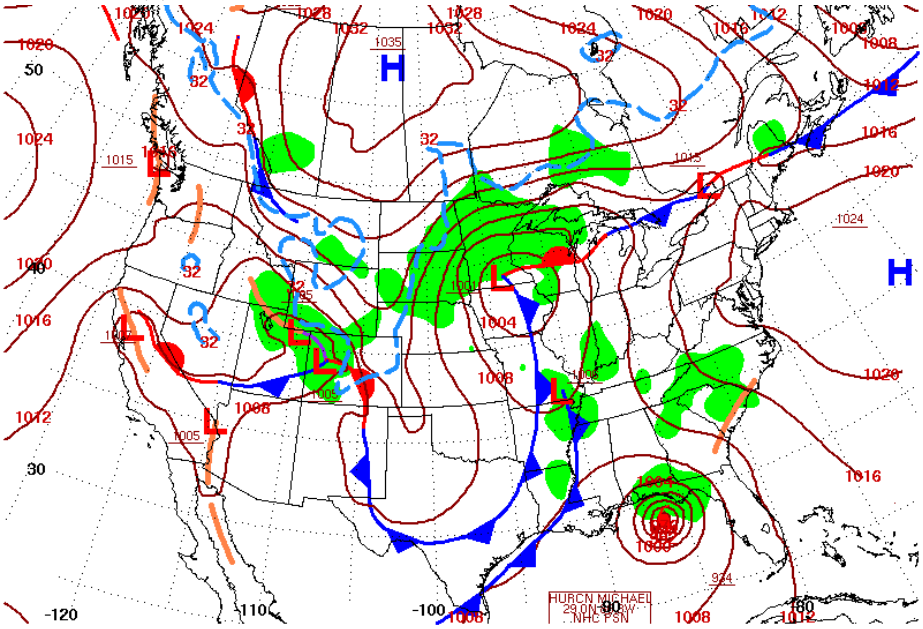

(b) Surface weather map analysis for 10 October 2018

Figure 24. Surface weather map analyses for 19 September and 10 October 2018. (a) Shows no significant weather to report in the Southeastern United States or Gulf of Mexico. (b) Shows Hurricane Michael in the Gulf of Mexico approaching the Florida coast and the cold front stretching across Louisiana into Texas. Courtesy of NOAA/National Centers for Environmental Prediction, Weather Prediction Center (2018).

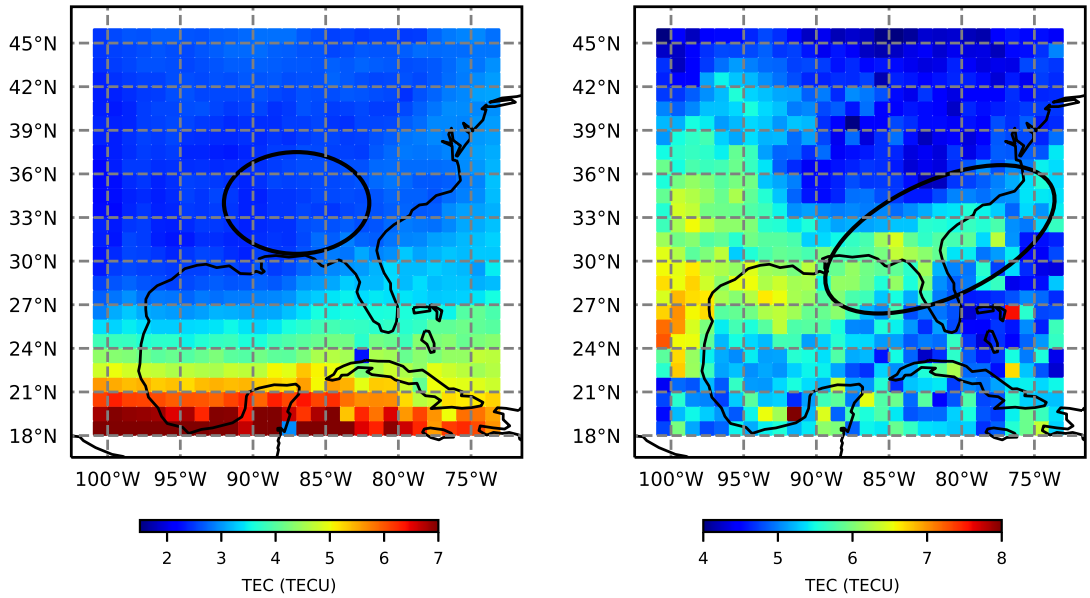

(a) Standard Deviation: 12 Sept

(b) Median: 12 Sept

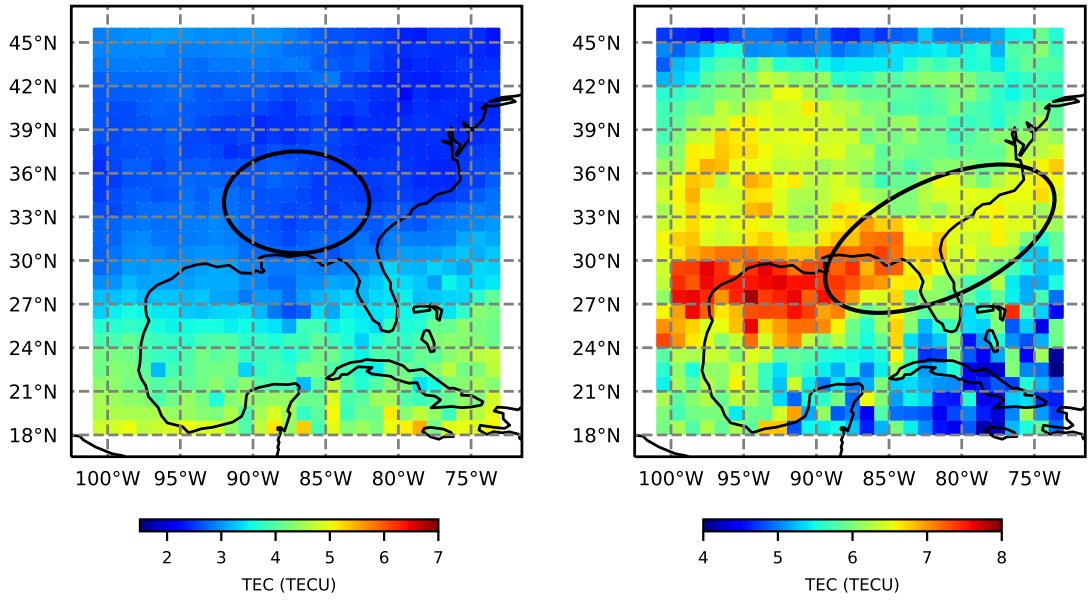

(c) Standard Deviation: 17 Sept

(d) Median: 17 Sept

Figure 25. Comparison of the standard deviation and median TEC for various days leading up to Hurricane Michael. It is not clear without further research why the TEC is greater than or equal to 7.0 TECU in (d) in the Northwestern Gulf of Mexico.

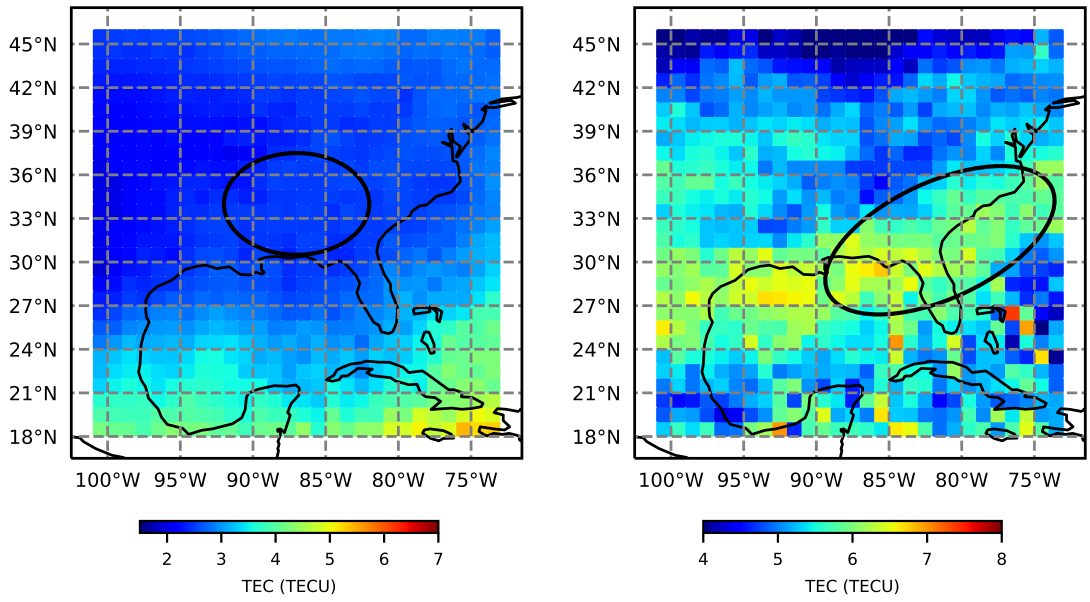

(a) Standard Deviation: 30 Sept

(b) Median: 30 Sept

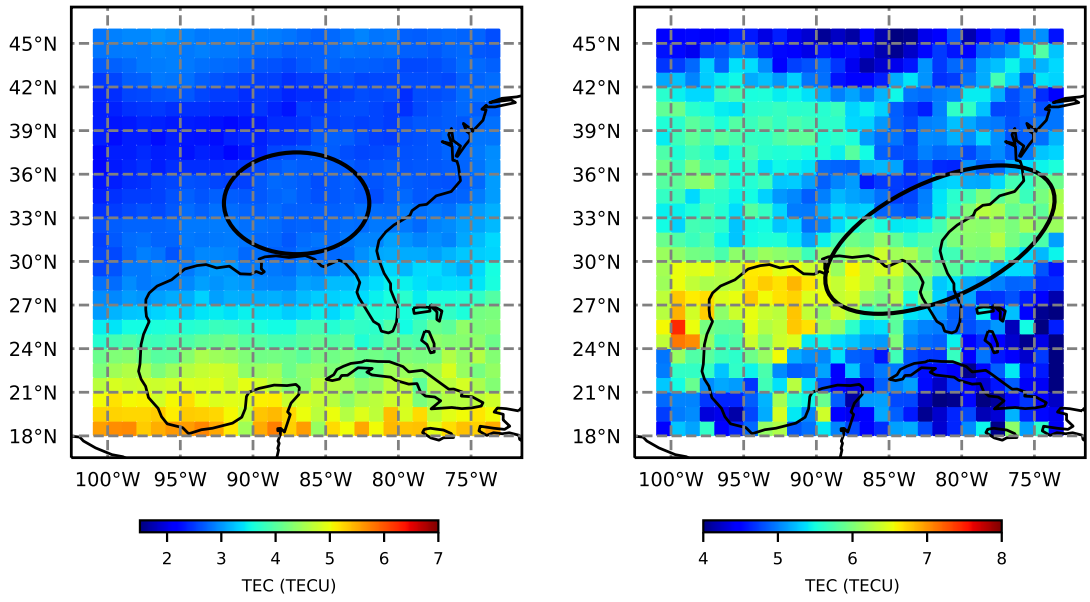

(c) Standard Deviation: 4 Oct

(d) Median: 4 Oct

Figure 26. Comparison of the standard deviation and median TEC for various days leading up to Hurricane Michael.

Bibliography

Beven II, J., Berg, R., and Hagen, A. (2019). Hurricane Michael (AL142018). Retrieved on 20 May 2019.

Chan, J. C. L. and Kepert, J. D. (2010). *Global Perspectives on Tropical Cyclones*, volume 4 of *World Scientific Series on Asia-Pacific Weather and Climate*. WORLD SCIENTIFIC.

Coster, A. (2019). World-wide Total Electron Content. `http://millstonehill.haystack.mit.edu/listExperiments/?isGlobal=on&categories=17&instruments=8000&showDefault=on&start_date_0=1950-01-01&start_date_1=00%3A00%3A00&end_date_0=2019-12-31&end_date_1=23%3A59%3A59`. Retrieved on 10 May 2019.

DiCiccio, T. J. and Efron, B. (1996). Bootstrap Confidence Intervals. *Statistical science*, pages 189–212.

Efron, B. and Tibshirani, R. (1986). Bootstrap Methods for Standard Errors, Confidence Intervals, and Other Measures of Statistical Accuracy. *Statistical science*, pages 54–75.

El-naggar, A. M. (2011). Enhancing the accuracy of GPS point positioning by converting the single frequency data to dual frequency data. *Alexandria Engineering Journal*, 50(3):237–243.

Goodman, S., Mach, D., Koshak, W., and Blakeslee, R. (2012a). GLM Lightning Cluster-Filter Algorithm. *Algorithm Theoretical Basis Document, Ver*, 3.

Goodman, S. J., Blakeslee, R., Mach, D., and Koshak, W. (2012b). The Geostationary Lightning Mapper (GLM) for the GOES-R Series of Geostationary Satellites.

Government Office for Science (2018). *Satellite-derived Time and Position: A Study of Critical Dependencies*. Government Office for Science, London.

Greenspan, M. and Yurick, M. (2003). Approximate kd tree search for efficient icp. In *Fourth International Conference on 3-D Digital Imaging and Modeling, 2003. 3DIM 2003. Proceedings.*, pages 442–448. IEEE.

Guha, A., Paul, B., Chakraborty, M., and De, B. K. (2016). Tropical Cyclone Effects on the Equatorial Ionosphere: First Result from the Indian Sector. *Journal of Geophysical Research: Space Physics*, 121(6):5764–5777.

Hegarty, C. J. and Chatre, E. (2008). Evolution of the Global Navigation Satellite System (GNSS). *Proceedings of the IEEE*, 96(12):1902–1917.

Huang, C. Y., Helmboldt, J., Park, J., Pedersen, T., and Willemann, R. (2019). Ionospheric detection of explosive events. *Reviews of Geophysics*, 57(1):78–105.

Immel, T. J., Mende, S. B., Hagan, M. E., Kintner, P. M., and England, S. L. (2009). Evidence of Tropospheric Effects on the Ionosphere. *Eos, Transactions American Geophysical Union*, 90(9):69–70.

Isaev, N., Kostin, V., Belyaev, G., Ovcharenko, O. Y., and Trushkina, E. (2010). Disturbances of the topside ionosphere caused by typhoons. *Geomagnetism and Aeronomy*, 50(2):243–255.

Ke, F., Wang, J., Tu, M., Wang, X., Wang, X., Zhao, X., and Deng, J. (2019). Characteristics and coupling mechanism of GPS ionospheric scintillation responses to the tropical cyclones in Australia. *GPS Solutions*, 23(2):34.

Landsea, C. (2014). Frequently Asked Questions. `https://www.aoml.noaa.gov/hrd/tcfaq/A15.html`. Accessed on 5 September 2019.

Landsea, C., Franklin, J., and Beven, J. (2015). The Revised Atlantic Hurricane Database (HURDAT2). *NOAA/NHC*.

Lay, E. H., Shao, X.-M., and Carrano, C. S. (2013). Variation in total electron content above large thunderstorms. *Geophysical Research Letters*, 40(10):1945–1949.

Leslie, J. and Bateman, J. (2018). Hurricane Michael Strengthens to a 'Potentially Catastrophic' Category 4 Storm. `https://www.nesdis.noaa.gov/content/hurricane-michael-strengthens-%E2%80%98potentially-catastrophic%E2%80%99-category-4-storm`. Accessed on 18 November 2019.

Lin, Y. and Mitchell, K. E. (2005). 1.2 the NCEP stage II/IV hourly precipitation analyses: Development and applications. In *19th Conf. Hydrology, American Meteorological Society, San Diego, CA, USA*. Citeseer. Retrieved on 19 November 2019.

Lonfat, M., Marks Jr, F. D., and Chen, S. S. (2004). Precipitation Distribution in Tropical Cyclones using the Tropical Rainfall Measuring Mission (TRMM) Microwave Imager: A Global Perspective. *Monthly Weather Review*, 132(7):1645–1660.

Molinari, J., Moore, P. K., Idone, V. P., Henderson, R. W., and Saljoughy, A. B. (1994). Cloud-to-ground lightning in Hurricane Andrew. *Journal of Geophysical Research: Atmospheres*, 99(D8):16665–16676.

National Centers for Environmental Prediction, Weather Prediction Center (2018). Daily Weather Maps. `https://www.wpc.ncep.noaa.gov/dailywxmap/index_20181010.html`. Accessed on 6 January 2020.

National Coordination Office for Space-Based Positioning, Navigation, and Timing

(2006). Public Safety and Disaster Relief. https://www.gps.gov/applications/safety/. Accessed on 11 February 2020.

National Coordination Office for Space-Based Positioning, Navigation, and Timing (2017). Other Global Navigation Satellite Systems (GNSS). https://www.gps.gov/systems/gnss/. Accessed on 31 May 2019.

National Geodetic Survey (2019). CORS Map. https://www.ngs.noaa.gov/CORS_Map/. Accessed on 18 November 2019.

NOAA Comprehensive Large Array-Data Stewardship System (2019). NOAA Comprehensive Large Array-Data Stewardship System. https://www.bou.class.noaa.gov/saa/products/search?sub_id=0&datatype_family=GRGLMPROD&submit.x=15&submit.y=7. Retrieved on 12 May 2019.

Polyakova, A. and Perevalova, N. (2011). Investigation into Impact of Tropical Cyclones on the Ionosphere using GPS Sounding and NCEP/NCAR Reanalysis Data. *Advances in Space Research*, 48(7):1196–1210.

Polyakova, A. and Perevalova, N. (2013). Comparative Analysis of TEC Disturbances over Tropical Cyclone Zones in the North–West Pacific Ocean. *Advances in Space Research*, 52(8):1416–1426.

Press, W. H. and Teukolsky, S. A. (1990). Savitzky-Golay Smoothing Filters. *Computers in Physics*, 4(6):669–672.

Rideout, W. and Coster, A. (2006). Automated GPS processing for global total electron content data. *GPS Solutions*, 10(3):219–228.

Savitzky, A. and Golay, M. J. (1964). Smoothing and Differentiation of Data by Simplified Least Squares Procedures. *Analytical chemistry*, 36(8):1627–1639.

Shultz, J. M., Russell, J., and Espinel, Z. (2005). Epidemiology of Tropical Cyclones: the Dynamics of Disaster, Disease, and Development. *Epidemiologic reviews*, 27(1):21–35.

Sickle, J. V. (2018). The Ionospheric Effect. `https://www.e-education.psu.edu/geog862/node/1715`. Accessed on 9 May 2019.

Space Weather Prediction Center (2018). GOES X-Ray Flux. `https://www.swpc.noaa.gov/products/goes-x-ray-flux`. Accessed on 20 November 2019.

Space Weather Prediction Center (2019a). Ionospheric Scintillation. `https://www.swpc.noaa.gov/phenomena/ionospheric-scintillation`. Accessed on 15 May 2019.

Space Weather Prediction Center (2019b). Total Electron Content. `https://www.swpc.noaa.gov/phenomena/total-electron-content`. Accessed on 15 May 2019.

Subirana, J. S., Zornoza, J. J., and Hernandez-Pajares, M. (2011). Ionospheric Delay. `https://gssc.esa.int/navipedia/index.php/Ionospheric_Delay`. Accessed on 24 September 2019.

Tascione, T. (2010). *Introduction to the Space Environment*. Orbit: A Foundation Series. Krieger Publishing Company.

Yu, B., Xue, X., Lu, G., Ma, M., Dou, X., Qie, X., Ning, B., Hu, L., Wu, J., and Chi, Y. (2015). Evidence for lightning-associated enhancement of the ionospheric sporadic e layer dependent on lightning stroke energy. *Journal of Geophysical Research: Space Physics*, 120(10):9202–9212.

REPORT DOCUMENTATION PAGE

Form Approved
OMB No. 0704–0188

1. REPORT DATE *(DD–MM–YYYY)*	2. REPORT TYPE	3. DATES COVERED *(From — To)*
26–03–2020	Master's Thesis	Oct 2018 — Mar 2020

4. TITLE AND SUBTITLE

LOCALIZED EFFECTS OF HURRICANE MICHAEL (2018) ON TOTAL ELECTRON CONTENT

5a. CONTRACT NUMBER

5b. GRANT NUMBER

5c. PROGRAM ELEMENT NUMBER

6. AUTHOR(S)

Williams, Joanna Eva Szewczyk, Capt, USAF

5d. PROJECT NUMBER

5e. TASK NUMBER

5f. WORK UNIT NUMBER

7. PERFORMING ORGANIZATION NAME(S) AND ADDRESS(ES)

Air Force Institute of Technology
Graduate School of Engineering and Management (AFIT/EN)
2950 Hobson Way
WPAFB OH 45433-7765

8. PERFORMING ORGANIZATION REPORT NUMBER

AFIT-ENP-MS-20-M-122

9. SPONSORING / MONITORING AGENCY NAME(S) AND ADDRESS(ES)

Undisclosed

10. SPONSOR/MONITOR'S ACRONYM(S)

11. SPONSOR/MONITOR'S REPORT NUMBER(S)

12. DISTRIBUTION / AVAILABILITY STATEMENT

DISTRIBUTION STATEMENT A:
APPROVED FOR PUBLIC RELEASE; DISTRIBUTION UNLIMITED.

13. SUPPLEMENTARY NOTES

14. ABSTRACT

Understanding the connection between terrestrial and space environments is an emerging field of study that can significantly improve different aspects of operational weather forecasting. In particular, it is well known that tropical cyclones (TCs) and thunderstorms can initiate gravity waves that generate fluctuations in the total electron content (TEC) of the ionosphere. These perturbations can deteriorate and delay the transmission of high-frequency (HF) communications used in emergency services, amateur radio, and aviation, for example. This study investigates changes in TEC according to the number of lightning flashes and the rainfall rates associated with Hurricane Michael (2018). A composite analysis is performed using the GOES Geostationary Lightning Mapper, NCEP Stage IV Precipitation, and MIT Haystack's GPS TEC data sets to characterize the influence of lightning on the ionosphere at Hurricane Michael's peak intensity on 10 October 2018. The techniques developed in this study have the potential to improve forecasting of tropical cyclogenesis, TC intensification, and the discrimination between naturogenic and anthropogenic phenomena impacts on the ionosphere.

15. SUBJECT TERMS

Tropical Cyclone, Ionosphere, Total Electron Content

16. SECURITY CLASSIFICATION OF:			17. LIMITATION OF ABSTRACT	18. NUMBER OF PAGES	19a. NAME OF RESPONSIBLE PERSON
a. REPORT	b. ABSTRACT	c. THIS PAGE			Lt Col Omar Nava, AFIT/ENP
U	U	U	U	80	19b. TELEPHONE NUMBER *(include area code)* (937) 255-3636, x4518; Omar.Nava@afit.edu